cancers

MDPI

Article

Targeted Lipidomic Profiling of Plasma-Derived Large Extracellular-Vesicle-Enriched Fractions in Lung Cancer

Said Naser [1], Matthias Schulz [1], Alexander C. Angleitner [1], Sven Schuchardt [2], Alexander von Hammerstein-Equord [3] and Judith Büntzel [1,*]

[1] Department of Hematology and Medical Oncology, University Medical Center Göttingen, 37075 Goettingen, Germany
[2] Fraunhofer-Institut für Toxikologie und Experimentelle Medizin ITEM, 30625 Hannover, Germany
[3] Department of Thoracic and Cardiovascular Surgery, University Medical Center Göttingen, 37075 Goettingen, Germany
* Correspondence: judith.buentzel@med.uni-goettingen.de

Simple Summary

Lung cancer remains a major cause of cancer-related death, and new blood-based markers are needed to better understand the disease and identify patients with different clinical outcomes. Extracellular vesicles are small membrane-covered particles released by cells into the bloodstream and can carry fats that reflect changes associated with cancer. We analyzed the lipid composition of blood fractions enriched for large extracellular vesicles from patients with non-small cell lung cancer, patients with small cell lung cancer, and healthy individuals. Patients with non-small cell lung cancer showed distinct changes in several ceramides and triglycerides. The lipid patterns also differed between non-small cell and small cell lung cancer, and selected lipids were associated with patient survival. These results provide new insight into lipid changes linked to lung cancer and identify candidates for future studies investigating blood-based markers for disease classification and patient outcome.

Abstract

Background/Objectives: Circulating extracellular-vesicle-enriched fractions may provide insight into cancer-associated metabolic alterations, but their lipid composition in non-small cell lung cancer remains insufficiently characterized. We aimed to identify lipid alterations in plasma-derived large extracellular vesicle (lEV)-enriched fractions from patients with non-small cell lung cancer, compare them with healthy controls and small cell lung cancer, and explore associations with clinicopathological characteristics and overall survival. **Methods**: lEV-enriched fractions were isolated from plasma samples of patients with non-small cell lung cancer (NSCLC, 74 enrolled; 73 included in lipidomic analyses), small cell lung cancer (SCLC, $n = 29$), and healthy controls ($n = 32$) by differential centrifugation. Lipids were quantified using targeted mass spectrometry. Group differences were assessed using multivariate analysis, differential abundance testing with false discovery rate correction, receiver operating characteristic analysis, survival analysis, and pathway enrichment. **Results**: NSCLC samples showed a distinct lipid pattern compared with controls, with 39 differentially abundant lipid species (31 increased, 8 decreased), including increased ceramides and triglycerides and decreased fatty acids. Cer(d18:2/16:0) (fold change 15.49; false discovery rate (FDR)-adjusted $p = 2.41 \times 10^{-33}$) and several triglycerides showed strong within-cohort separation between non-small cell lung cancer and controls (area under the curve (AUC) 0.973 for Cer(d18:2/16:0)). Selected lipids were associated with overall survival in exploratory analyses (hazard ratio (HR) 2.39; 95% confidence interval

Check for updates

Academic Editor: Ole Hilberg

Received: 29 October 2026
Revised: 16 November 2026
Accepted: 20 November 2026
Published: 29 November 2026

Copyright: © 2026 by the authors. Licensee MDPI, Basel, Switzerland. This article is an open access article distributed under the terms and conditions of the Creative Commons Attribution (CC BY) license.

(CI) 1.08–5.31 for Cer(d18:2/16:0)). Lipid profiles differed markedly between NSCLC and SCLC, whereas adenocarcinoma and squamous cell carcinoma showed broadly overlapping patterns. Sphingolipid-related pathways were enriched in NSCLC. **Conclusions**: Plasma-derived lEV-enriched fractions contain distinct lung-cancer-associated lipid patterns. These findings support further validation of selected lipids as candidate markers of lung cancer subtype and clinical outcome.

Keywords: large extracellular vesicles; lipidomics; non-small cell lung cancer; small cell lung cancer; liquid biopsy; ceramides; targeted mass spectrometry

1. Introduction

Non-small cell lung cancer (NSCLC), the predominant histological type of lung cancer, remains a major cause of cancer-related mortality. Lung cancer was the leading cause of cancer-related death worldwide in 2024, accounting for approximately 1.9 million deaths, while approximately 58,300 new cases were reported in Germany in 2023 [1–3]. Major risk factors include tobacco smoke exposure and environmental or occupational hazards, such as radon, asbestos, and air pollution [2]. In addition, immune evasion through the programmed cell death protein 1/programmed death-ligand 1 (PD-1/PD-L1) axis contributes to tumor progression and provides the biological basis for the use of immune checkpoint inhibitors [4,5]. Because early-stage disease is frequently asymptomatic, NSCLC is often diagnosed at an advanced stage [6]. To facilitate earlier detection, current guidelines recommend low-dose computed tomography screening for eligible individuals at high risk of lung cancer [7].

Liquid biopsy approaches have gained increasing attention as minimally invasive tools for the molecular characterization and monitoring of cancer [8]. However, their broad clinical implementation remains limited by pre-analytical variability and incomplete standardization across analytical workflows [9,10]. Among circulating analytes, extracellular vesicles (EVs) represent a biologically active source of biomarker information because they carry proteins, lipids, and nucleic acids and contribute to intercellular communication [11,12]. According to the Minimal Information for Studies of Extracellular Vesicles (MISEV) recommendations, EV subtypes should primarily be described using operational terms based on their physical characteristics, enrichment procedures, and molecular characterization. Their classification should not rely on presumed biogenesis alone [10,13]. EVs can originate from the endosomal pathway, giving rise to exosomes, or through outward budding of the plasma membrane, generating ectosomes. However, these biogenesis-based subtypes overlap in size, and the distinction between small extracellular vesicles (sEVs) and large extracellular vesicles (lEVs) does not establish their subcellular origin. lEVs are commonly distinguished from sEVs using an operational size threshold of approximately 200 nm, although their size distributions may overlap. lEV-enriched fractions can be obtained from peripheral blood plasma by differential centrifugation, while alternative enrichment approaches include size-exclusion chromatography and density-gradient centrifugation. EV characterization commonly involves particle size analysis, imaging techniques, and assessment of EV-associated protein markers. This makes lEV-enriched fractions accessible for translational molecular profiling studies [12–14]. In cancer, EVs can exert context-dependent effects by promoting tumor progression, immune evasion, and metastasis, while under certain conditions also contributing to antitumor immune responses [11,15].

In NSCLC, increased concentrations of circulating EVs or exosomes have been associated with clinicopathological characteristics and clinical outcome [16]. However, bulk EV

measurements are influenced by biological and pre-analytical factors and therefore have limited tumor specificity when used as abundance-based readouts alone [17–19]. Consequently, increasing attention has shifted toward the molecular profiling of EV-associated cargo. For example, exosomal PD-L1 measurements have been linked to immune checkpoint inhibitor response and clinical outcome [20,21]. In addition, EV-derived nucleic acids have been investigated for tumor genotyping in liquid biopsy samples, including epidermal growth factor receptor testing in NSCLC [22]. Beyond their diagnostic potential [23], EVs are also being investigated as therapeutic delivery vehicles and for immunomodulatory applications in cancer treatment [15]. Despite extensive research on EVs in NSCLC, metabolomic and lipidomic analyses of circulating EV-enriched fractions remain comparatively limited [24–26].

In our previous study, targeted metabolomic profiling of plasma-derived lEV-enriched fractions from patients with small cell lung cancer (SCLC) revealed distinct metabolite patterns compared with healthy controls and suggested associations between selected lipid species and clinical outcome [27]. However, the lipid composition of plasma-derived lEV-enriched fractions in NSCLC and potential entity-associated differences between NSCLC and SCLC remain insufficiently characterized. Building on these findings, the present proof-of-concept study used targeted-mass-spectrometry-based profiling with the MxP® Quant 500 platform to characterize the lipid profiles of plasma-derived lEV-enriched fractions in NSCLC. Specifically, we aimed to (i) identify lipid species that differed between patients with NSCLC and healthy controls, (ii) compare lipid profiles of lEV-enriched fractions between NSCLC and SCLC to explore entity-associated patterns, and (iii) investigate associations with clinicopathological characteristics and overall survival in a hypothesis-generating manner.

2. Materials and Methods

2.1. Patient Recruitment and Clinical Data

This study was designed as a single-center observational biomarker study with prospective sample collection and retrospective lipidomic analysis. The study was approved by the local Ethics Committee of the University Medical Center Göttingen (approval no. 3/2/14; approval date: 17 March 2014) and was conducted in accordance with the Declaration of Helsinki. Written informed consent was obtained from all participants prior to inclusion.

Adult patients with histologically confirmed NSCLC were recruited at the University Medical Center Göttingen, Germany, between November 2013 and February 2021. Histological classification, including the diagnosis of lung adenocarcinoma (LUAD) and lung squamous cell carcinoma (LUSC), was performed by board-certified pathologists as part of routine clinical diagnostics according to World Health Organization criteria. The cohort included patients with stage III or IV disease requiring systemic therapy and reflected a clinically heterogeneous real-world population, including patients at initial diagnosis as well as patients with recurrent disease. Blood samples were collected before surgery, radiotherapy, or systemic anticancer treatment whenever applicable, or during treatment-free intervals, in order to minimize the influence of therapy-induced apoptotic bodies on the lEV-enriched fraction. In selected patients with stable disease during maintenance treatment, blood sampling was performed during routine clinical follow-up. Stable disease was assessed according to standard-of-care radiological evaluation in clinical routine. Maintenance treatment included immune checkpoint inhibition, pemetrexed-based maintenance therapy, or tyrosine kinase inhibitor treatment, depending on the underlying tumor biology and clinical indication. Only one plasma sample per patient was included in the present analysis.

Patients with a second active malignancy or without written informed consent were excluded. Overall, 74 patients with NSCLC were included. Of these, 73 samples were

available in the final lipidomic analysis dataset, while one sample was not included in the lipidomic analyses. The study was exploratory; therefore, no formal sample-size calculation was performed. The allocation of NSCLC samples relative to the combined comparator cohorts was guided by available prospectively collected samples, analytical feasibility, and the expected clinical distribution of lung cancer entities. NSCLC represents the majority of lung cancer cases.

A comparative cohort of 29 adult patients with histologically confirmed extensive-stage SCLC, recruited at the same center between March 2014 and March 2021, was included to explore entity-associated lipidomic differences. Details of this cohort have been reported previously [27]. SCLC samples were collected, processed, and analyzed using the same pre-analytical and lipidomic workflow as the NSCLC samples, and measurements were performed within the same analytical batch. The same healthy control cohort was used for the NSCLC and SCLC comparisons.

Healthy controls ($n = 32$) were recruited between November 2013 and May 2020 from hospital staff, healthy volunteers, and regular blood donors. Controls had no known history of malignancy and no relevant acute disease at the time of blood collection. Minor chronic conditions, such as treated arterial hypertension, were not considered exclusion criteria. Controls were sex-balanced but were not age-matched to the lung cancer cohorts. For a subset of healthy controls recruited through blood donation, only age and sex were available, limiting the assessment of additional clinical and lifestyle-related characteristics. Blood samples from patients and controls were collected under non-fasting conditions and processed according to the same protocol. Demographic and baseline clinical characteristics of the study cohorts are summarized in Tables 1 and 2.

Table 1. Clinical characteristics of the overall NSCLC cohort and controls.

Clinical Characteristics NSCLC Patients	
Age median (patients, min–max range)	62.4 (43.8–82.9) years
Body mass index median (time blood sample drawn, min–max range)	23.6 (16.9–34.5) kg/m^2
Sex	
Male	41/74
Female	33/74
Cancer subtype	
LUAD	49/74
LUSC	13/74
n/A	12/74
Metastasis	
Single or no metastasis (≤1 metastasis)	35/68
Polymetastasis (>1 metastasis)	33/68
Location of metastasis (N locations)	
Bone	24/101
Brain	39/101
Liver	13/101
Lung	14/101
Other	11/101
Stable vs. progressive disease	
Stable	30/57
Progressive	27/57
Baseline Characteristics Controls	
Age median (controls, min–max range)	43 (20–64)
Sex	
Male	16
Female	16

Max: maximum; min: minimum; n/A: no information available; NSCLC: non-small cell lung cancer; LUAD: lung adenocarcinoma; LUSC: lung squamous cell carcinoma.

Table 2. Clinical characteristics of SCLC patients.

Clinical Characteristics SCLC Patients	
Age median (patients, min–max range)	62.4 (49.0–79.2) years
Body mass index median (time blood sample drawn, min–max range)	23.3 (17.9–30.1) kg/m^2
Sex	
Male	17/29
Female	12/29
Metastasis	
Single or no metastasis (≤1 metastasis)	13/27
Polymetastasis (>1 metastasis)	14/27
Location of metastasis (N metastasis)	
Bone	8/27
Brain	19/27
Liver	7/27
Lung	4/27
Other	3/27
TTF-1 expression	
Positive	20/29
Negative	9/29

Max: maximum; min: minimum; SCLC: small cell lung cancer; TTF-1: thyroid transcription factor.

Clinical data were obtained from the electronic medical records and the institutional oncology documentation system. Recorded variables included age, sex, body mass index, histological subtype, tumor stage, metastatic status, treatment context at blood sampling, tumor programmed death-ligand 1 expression, and survival status. PD-L1 expression was assessed as a tumor proportion score (TPS) in routine pathology. Overall survival was defined as the time from initial lung cancer diagnosis to death from any cause or last documented follow-up. An overview of the study design, sample processing, and analytical workflow is provided in Supplementary Figure S1.

2.2. Plasma Processing and Enrichment of lEV-Enriched Fractions

Peripheral blood (15 mL) was collected into ethylenediaminetetraacetic acid (EDTA)-containing tubes (#8076.3, Carl Roth, Karlsruhe-Mühlburg, Germany) and processed within 2 h after blood draw. Plasma was obtained by centrifugation at 1200× *g* for 15 min at room temperature. Plasma was then subjected to sequential differential centrifugation to enrich a medium/lEV-containing extracellular particle fraction, following a previously established differential centrifugation workflow [28] and using operational EV terminology in line with MISEV recommendations [10,13].

Briefly, plasma was centrifuged at 1500× *g* for 15 min to remove residual cells, cellular debris, and larger contaminants. The resulting supernatant was transferred to fresh centrifugation tubes and centrifuged at 14,000× *g* for 35 min at 4 °C to pellet the lEV-enriched fraction. After removal of the supernatant, pellets were washed once with phosphate-buffered saline (PBS; AC-BS-0002, Anprotec, Bruckberg, Germany) and centrifuged again at 14,000× *g* for 35 min at 4 °C. The final pellets were resuspended in PBS. Because the final resuspension volume varied slightly due to manual sample processing, downstream analyses were normalized by total protein content rather than by resuspension volume.

Total protein content of the lEV-enriched preparations was quantified by Lowry assay. In line with the previously established workflow for blood-derived lEVs/microvesicles, total protein content was used as a pragmatic surrogate measure for vesicle-enriched particle input and for normalization across samples [28]. In that previous study, particle numbers and estimated vesicle surface area normalized to 50 µg of protein did not differ significantly between cancer patients and healthy controls (Figure 1c and Appendix Figure A1 in [28]).

Because systematic particle-count measurements were not available for all samples in the present cohort, protein-based normalization was used for downstream lipidomic profiling. For lipidomic profiling, 50 µg of protein from each lEV-enriched preparation was used per sample. Aliquots were stored at −20 °C until lipidomic analysis. The resulting preparations were further assessed by Western blotting and representative nanoparticle tracking analysis (NTA), as described below.

2.3. Western Blot Analysis

Protein expression in human plasma and lEV-enriched preparations was examined by immunoblotting. Briefly, equal amounts of protein (17 µg per lane) were separated by sodium dodecyl sulfate polyacrylamide gel electrophoresis (SDS-PAGE; #0183.1, Carl Roth, Karlsruhe-Mühlburg, Germany) and transferred onto nitrocellulose membranes. Membranes were blocked in Tris-buffered saline with Tween-20 (TBST; 137 mM NaCl (#3957.2, Carl Roth, Karlsruhe-Mühlburg, Germany), 20 mM Tris (#10376743, Fisher Scientific, Waltham, MA, USA), pH 7.6, 0.1% [v/v] Tween-20 (#A4974,0250, AppliChem GmbH, Darmstadt, Germany)). They were subsequently incubated overnight at 4 °C with primary antibodies against α-ACTININ-4 (sc-390205), APOLIPOPROTEIN A-I (APOA1, sc-376818), β-ACTIN (sc-47778), and RAC-GTPase-ACTIVATING PROTEIN 1 (RGAP1, sc-271110; all Santa Cruz Biotechnology, Dallas, TX, USA). After three washes in TBST (3 × 5 min), membranes were incubated with a horseradish peroxidase-conjugated secondary antibody (#7076, Cell Signaling Technology, Danvers, MA, USA) at room temperature, followed by another series of TBST washing steps (3 × 5 min). Bands were visualized using ECL Prime chemiluminescent substrate (GE Healthcare, Chicago, IL, USA) and documented with a LAS-4000 imaging system (Fujifilm, Düsseldorf, Germany). Ponceau S staining (#A2935,0500, Th. Geyer, Renningen, Germany) was routinely performed as a loading control.

Western blotting was used to assess vesicle-associated proteins and potential co-enriched plasma components in the lEV-enriched preparations. APOA1 was included as a marker of lipoprotein-associated material. These analyses supported the characterization of the enriched extracellular particle fraction but were not intended to demonstrate purity or tumor-specific vesicle origin.

2.4. Nanoparticle Tracking Analysis

Representative NTA of lEV-enriched preparations was performed using a ZetaView PMX-120 instrument (PMX 120 ZetaView® Mono Laser, Particle Metrix, Inning am Ammersee, Germany) equipped with a 640 nm laser and a complementary metal-oxide-semiconductor camera (640 × 480 pixels; Particle Metrix). Measurements were performed in five healthy control preparations ($n = 5$) as a proof-of-principle assessment of particle size distribution and concentration. Samples were diluted in PBS to achieve a suitable measurement range of approximately 50–400 particles per frame. For each preparation, videos were recorded at 11 cell positions at 25 °C. Data were processed and analyzed using ZetaView software (version 8.02.31, ZetaView® Inning am Ammersee, Germany), yielding particle size distributions and particle concentrations.

NTA was not performed systematically for all patient and control samples; therefore, particle counts were not used for normalization in the present study. NTA and Western blot analyses were intended to characterize the established enrichment workflow rather than to serve as individual quality control assessments of each preparation. All patient and control samples underwent the same differential centrifugation and washing procedures, followed by protein-based normalization, ensuring a standardized processing workflow across cohorts. Together with Western blot-based marker assessment, representative NTA

supported the presence of extracellular particles compatible with lEV-enriched preparations. However, the analyzed material should be interpreted as a plasma-derived lEV-enriched extracellular particle fraction rather than as a purified, quantitatively particle-normalized, or tumor-specific EV population.

2.5. Lipid Extraction and Targeted Mass Spectrometry

For lipidomic profiling of plasma-derived lEV-enriched fractions, 50 µg of protein-normalized material was mixed with 30 µL of methanol/water (9:1, *v*/*v*, methanol—#P717.1 Carl Roth, Karlsruhe-Mühlburg, Germany). The samples were subjected to three freeze–thaw cycles at −150 °C to disrupt vesicle membranes, as previously described [28]. Ten microliters of each lysed sample was used for subsequent targeted mass spectrometry-based analysis.

Targeted metabolite and lipid measurements were performed using the MxP® Quant 500 kit according to the manufacturer's instructions (Biocrates Life Sciences AG, Innsbruck, Austria). This commercial kit enables the simultaneous quantification of up to 630 metabolites across 14 small molecule classes and 12 lipid classes. As small molecule coverage was insufficient after filtering in the present lEV-enriched fraction dataset, the present analysis focused on lipid species. The analytical workflow combines flow injection analysis tandem mass spectrometry (FIA-MS/MS) for broad lipid class coverage and liquid chromatography tandem mass spectrometry (LC-MS/MS) for small molecules. LC-MS/MS was performed on an Agilent 1290 Infinity II liquid chromatography system (Agilent Technologies, Santa Clara, CA, USA) coupled to a SCIEX 5500 QTrap mass spectrometer (SCIEX, Darmstadt, Germany) operating in multiple reaction monitoring (MRM) mode. All samples included in the comparative analyses were measured within the same analytical batch. Calibration standards, internal standards, and quality control samples were processed according to the manufacturer's instructions.

Data acquisition and peak integration were performed using SCIEX Analyst software (Version 1.7, CIEX Framingham/Marlborough, MA, USA). The resulting data were imported into Biocrates MetIDQ software (Oxygen version Biocrates Life Sciences AG, Innsbruck, Austria) for analyte identification and concentration calculation according to the manufacturer's workflow. For downstream statistical analyses, metabolites were retained only if concentrations were above the limit of detection or quantification in at least 50% of samples in at least one of the groups included in the respective comparison. Metabolites not meeting this criterion were excluded from the corresponding analysis.

2.6. Statistical Analysis and Bioinformatics

Statistical analyses were performed using MetaboAnalyst 6.0 and GraphPad Prism (version 9.0; GraphPad Software, La Jolla, CA, USA [29]). Concentration data generated by Biocrates MetIDQ were used for downstream analyses. Lipid species were retained for a given group comparison only if concentrations were above the limit of detection or quantification in at least 50% of samples in at least one of the groups included in the respective comparison. Lipids not meeting this criterion were excluded from the corresponding analysis.

Data were explored by principal component analysis (PCA) and hierarchical clustering heatmaps to visualize cohort-level differences in lipid profiles. For multivariate visualization, data were processed in MetaboAnalyst using log transformation and Pareto scaling unless otherwise indicated. Hierarchical clustering heatmaps were generated from normalized lipid abundance data to illustrate group-associated patterns. Univariate group comparisons were performed using two-sided tests selected according to the analysis objective and data characteristics. Fold changes and volcano plots were used to summarize the direction and magnitude of lipid abundance differences. A nominal significance threshold of $p < 0.05$

was applied for exploratory analyses. False discovery rate (FDR) correction was performed using the Benjamini–Hochberg procedure where indicated [30]. Differential lipid species were interpreted primarily on the basis of FDR-corrected results and biological plausibility.

To assess shared and distinct lipid alterations across entities and histological subgroups, lists of differential lipid species derived from the NSCLC-, SCLC-, LUAD, and LUSC-versus-control comparisons were compared and visualized using a Venn diagram.

Receiver operating characteristic (ROC) analyses were performed as exploratory measures of within-cohort separation for individual lipids in this dataset. Area under the curve (AUC) values with 95% confidence intervals (CIs) were calculated where applicable. ROC-derived separation metrics were interpreted as descriptive measures of group separation within the present cohort and not as evidence of clinical diagnostic performance, as no independent validation cohort was available [31]. Exploratory internal validation of lipid-based discrimination was performed using repeated stratified five-fold cross-validation (100 repetitions) and bootstrap-based optimism correction (2000 resamples). To account for potential selection-related optimism, the best-performing lipid was selected from 117 candidate analytes based on training-set AUC within each cross-validation fold or bootstrap sample. Discrimination was assessed using the AUC, and bootstrap optimism was estimated as the mean difference between performance in bootstrap samples and performance in the original dataset.

Overall survival analyses were conducted in a hypothesis-generating manner. Overall survival was defined as the time from initial lung cancer diagnosis to death from any cause or last documented follow-up. Patients were stratified into high and low lipid groups for visualization using X-tile to derive data-driven cutoffs within this dataset [32]. Survival curves were plotted using Kaplan–Meier estimates and compared using the log-rank test. Hazard ratios (HRs) with 95% confidence intervals were calculated using Cox proportional hazards models. Because of the exploratory design, limited sample size, and data-driven cutoff selection, survival associations were interpreted as preliminary and require independent validation.

Pathway enrichment analysis was performed using the LIPEA web service and the MetaboAnalyst "Pathway Analysis" module [29,33]. Significantly altered lipids were mapped to Kyoto Encyclopedia of Genes and Genomes (KEGG) identifiers [34,35]. Multiple-testing correction for pathway-level analyses was performed using Benjamini–Hochberg adjustment, with adjusted $p < 0.05$ considered significant. Pathway results were interpreted cautiously because only lipids that could be mapped to KEGG identifiers contributed to the enrichment analysis.

3. Results

3.1. Clinical Characteristics and Characterization of the lEV-Enriched Fraction

Clinical characteristics of the NSCLC cohort and healthy controls are summarized in Table 1, and characteristics of the SCLC cohort and controls are summarized in Table 2. The NSCLC cohort comprised 74 patients and was predominantly male (41/74). Lipidomic analyses were performed using 73 NSCLC samples. Most NSCLC patients presented with metastatic disease at the time of sampling.

Plasma-derived lEV-enriched fractions were characterized by representative NTA and Western blotting (Figure 1). NTA performed in healthy control preparations ($n = 5$) demonstrated particle-containing fractions with a size distribution compatible with enrichment of extracellular particles in the expected size range of the applied differential centrifugation protocol. Western blot analysis was used to assess vesicle-associated proteins and potential co-enriched plasma components in plasma and lEV-enriched preparations. β-ACTIN was clearly detectable in the three patient-derived preparations, whereas α-ACTININ-4 and

RGAP1 signals could not be reliably identified in all patient lanes. APOA1 was included to assess lipoprotein-associated co-enrichment and was not detectable in the analyzed patient-derived preparations. Together, these analyses supported the enrichment of an lEV-containing extracellular particle fraction. However, because NTA was performed as representative proof-of-principle characterization and not systematically across all study samples, the analyzed material should be interpreted as a plasma-derived lEV-enriched fraction rather than as a purified or tumor-specific EV population.

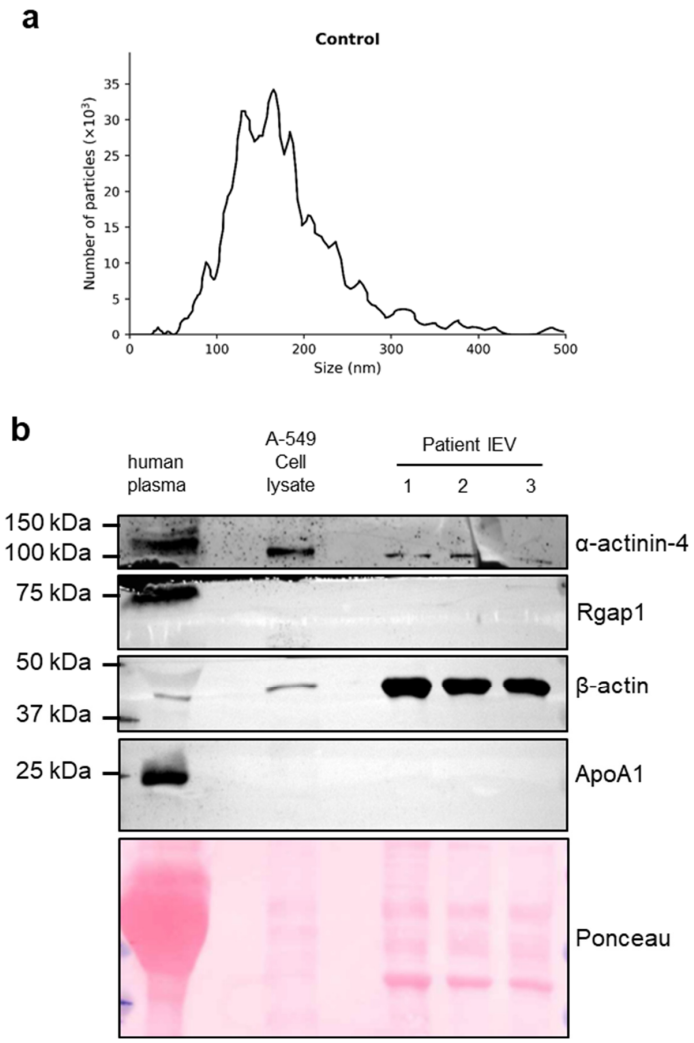

Figure 1. Representative characterization of plasma-derived large extracellular vesicle (lEV)-enriched fractions. (**a**) Representative nanoparticle tracking analysis (NTA) of healthy control preparations ($n = 5$) demonstrated particle-containing fractions with a size distribution compatible with enrichment of extracellular particles in the expected size range of the applied differential centrifugation protocol. The plot shows particle number according to particle size. (**b**) Western blot analysis of human plasma and lEV-enriched preparations was performed to assess proteins previously used in the established lEV-enrichment workflow and potential co-enriched plasma components. α-ACTININ-4, RGAP1, and β-ACTIN were assessed as vesicle-associated/cytoskeletal markers, whereas APOA1 was included as a marker of lipoprotein-associated material. Ponceau S staining served as a loading control. β-ACTIN bands were clearly detectable in all three patient-derived preparations, whereas α-ACTININ-4 and RGAP1 signals could not be reliably identified in all patient lanes. The Western blot findings were interpreted qualitatively, without conclusions regarding relative protein abundance or the quantitative degree of EV enrichment. NTA was performed as representative proof-of-principle characterization and was not used for particle-count-based normalization of the lipidomic dataset. The original Western blot figures can be found in Figure S5.

3.2. lEV-Enriched Fractions Show a Distinct NSCLC-Associated Lipid Pattern

Targeted lipidomic profiling of plasma-derived lEV-enriched fractions revealed cohort-level differences between NSCLC patients and healthy controls. PCA showed partial separation of NSCLC and control samples (Figure 2a). Hierarchical clustering of differentially abundant analytes supported group-associated lipid patterns (Figure 2b). Univariate differential abundance testing identified 39 altered lipid species in NSCLC compared with controls, including 31 species with increased and 8 decreased abundance based on the predefined criteria (Figure 3a). Detailed results are summarized in Table 3.

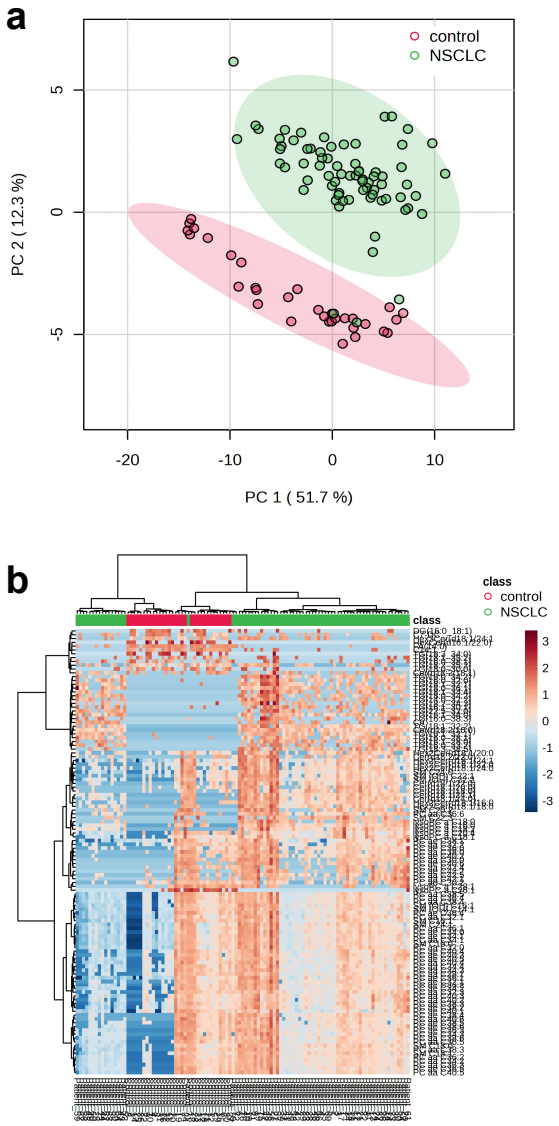

Figure 2. Cohort-level separation of plasma-derived large extracellular vesicle (lEV)-enriched lipid profiles in NSCLC patients and healthy controls. (**a**) Principal component analysis (PCA) of targeted lipidomic data from plasma-derived lEV-enriched fractions. Each dot represents one sample. The first two principal components accounted for 51.7% and 12.3% of the total variance, respectively. The score plot shows partial separation between NSCLC patients ($n = 73$) and healthy controls ($n = 32$), indicating cohort-associated differences in lipid composition. Ellipses indicate the distribution of the respective sample groups. (**b**) Hierarchical clustering heatmap of lipid abundances in NSCLC and control samples. Columns represent individual samples and rows represent lipid species. Values are shown as normalized relative abundances, with red indicating higher and blue indicating lower abundance. The heatmap provides an overview of cohort-associated lipid patterns rather than a detailed visualization of individual lipid species.

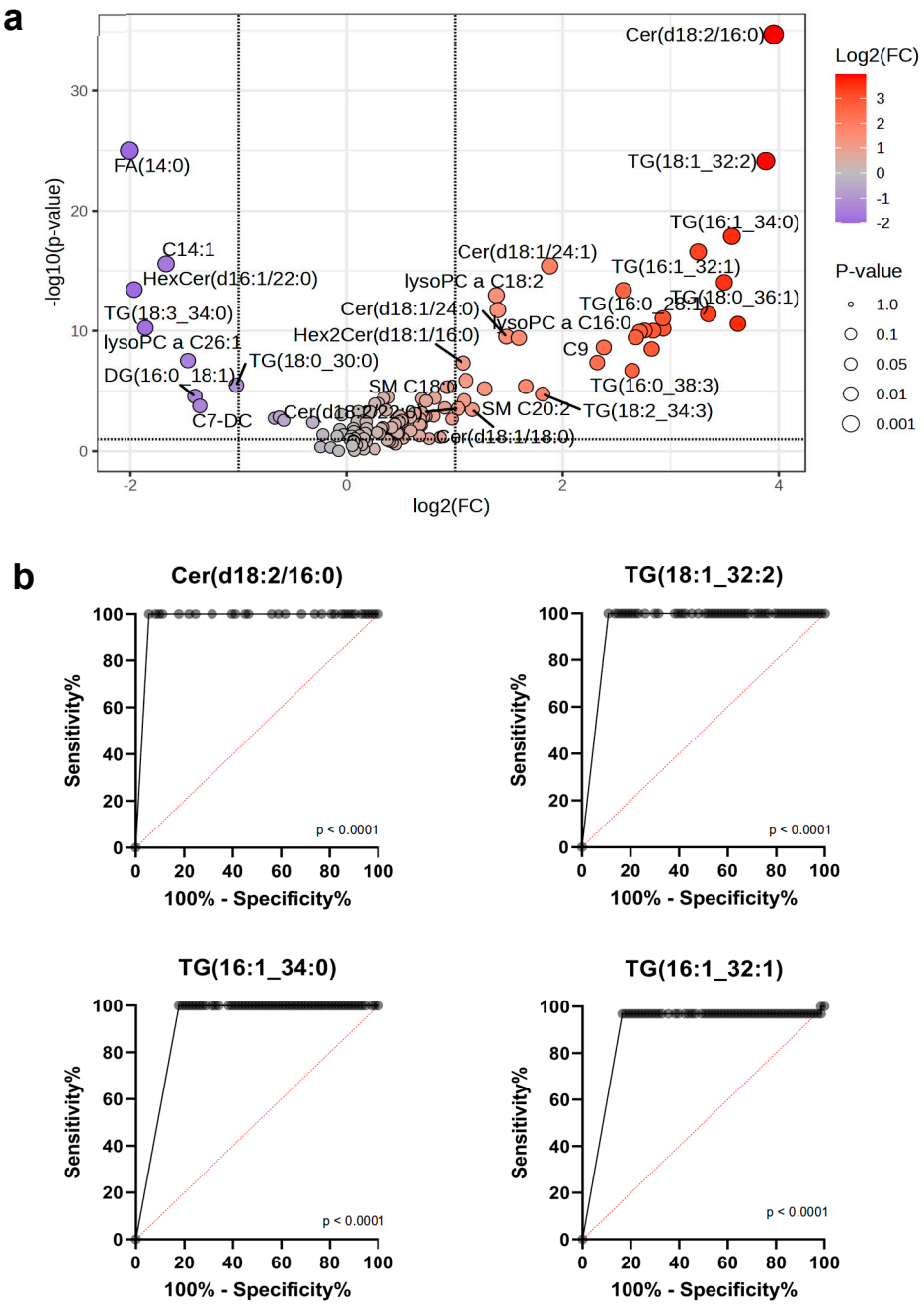

Figure 3. Differential lipid abundance and exploratory within-cohort separation of selected lipid species in NSCLC and healthy controls. (**a**) Volcano plot showing differential lipid abundance in plasma-derived large extracellular vesicle (lEV)-enriched fractions from NSCLC patients compared with healthy controls. The x-axis shows log2 fold change, and the y-axis shows −log10 raw *p*-value. Lipids with higher abundance in NSCLC are shown on the right, whereas lipids with lower abundance in NSCLC are shown on the left. Dot color indicates log2 fold change, and dot size indicates *p*-value. Prominent altered lipid species included increased Cer(d18:2/16:0) and several triglycerides, as well as decreased FA(14:0) and C14:1. FDR-adjusted statistical results are provided in Table 3. (**b**) Exploratory receiver operating characteristic curves for selected lipid species illustrating within-cohort separation between NSCLC patients (n = 73) and controls (n = 32). Area under the curve (AUC) values with 95% confidence intervals (CI) are shown for each lipid. These analyses were performed as descriptive separation metrics within the present cohort and do not represent validated clinical diagnostic performance.

Table 3. Distinct metabolites of large extracellular vesicles in NSCLC patients compared to healthy controls, FDR ≤ 0.05.

Metabolite	Fold Change	Log2 (Fold Change)	*p*-Value, FDR Corrected.
Cer(d18:2/16:0)	15.489	3.9531	2.4135×10^{-33}
FA(14:0)	0.24817	−2.0106	6.10×10^{-24}
TG(18:1_32:2)	14.734	3.881	2.95×10^{-23}
TG(16:1_34:0)	11.848	3.5665	4.04×10^{-17}
TG(16:1_32:1)	9.5432	3.2545	6.35×10^{-16}
C14:1	0.31413	−1.6706	5.29×10^{-15}
Cer(d18:1/24:1)	3.6799	1.8797	6.84×10^{-15}
TG(18:0_36:1)	11.284	3.4962	1.36×10^{-13}
HexCer(d16:1/22:0)	0.256	−1.9658	4.78×10^{-13}
TG(16:0_28:1)	5.9022	2.5613	4.93×10^{-13}
lysoPC a C18:2	2.6169	1.3879	1.17×10^{-12}
lysoPC a C16:0	2.6408	1.401	1.82×10^{-11}
TG(16:1_28:0)	10.183	3.3481	3.67×10^{-11}
TG(18:0_34:2)	7.616	2.929	7.41×10^{-11}
TG(16:0_34:2)	12.313	3.6221	2.03×10^{-10}
TG(18:3_34:0)	0.27499	−1.8626	4.14×10^{-10}
TG(18:3_38:5)	7.6308	2.9318	4.47×10^{-10}
TG(16:0_32:0)	7.1531	2.8386	5.91×10^{-10}
TG(14:0_32:2)	6.7654	2.7582	5.91×10^{-10}
TG(18:1_32:1)	6.5662	2.715	6.93×10^{-10}
Cer(d18:1/24:0)	2.7904	1.4805	1.67×10^{-9}
TG(22:5_32:0)	6.3993	2.6779	1.86×10^{-9}
Hex2Cer(d18:1/18:0)	3.022	1.5955	1.99×10^{-9}
TG(16:0_33:2)	5.2084	2.3808	1.18×10^{-8}
TG(18:1_34:4)	7.0835	2.8245	1.52×10^{-8}
lysoPC a C26:1	0.36128	−1.4688	1.37×10^{-7}
C9	4.9929	2.3199	1.92×10^{-7}
Hex2Cer(d18:1/16:0)	2.1115	1.0783	2.05×10^{-7}
TG(16:0_38:3)	6.2476	2.6433	8.16×10^{-7}
SM C18:0	2.15	1.1043	5.26×10^{-6}
TG(18:0_30:0)	0.49352	−1.0188	1.28×10^{-5}
TG(16:1_30:1)	3.1576	1.6588	1.56×10^{-5}
lysoPC a C18:0	2.4284	1.28	2.30×10^{-5}
TG(18:2_34:3)	3.5191	1.8152	6.18×10^{-5}
DG(16:0_18:1)	0.3776	−1.4051	9.16×10^{-5}
SM C20:2	2.1259	1.0881	1.80×10^{-4}
C7-DC	0.38984	−1.359	4.63×10^{-4}
Cer(d18:2/22:0)	2.0456	1.0325	7.27×10^{-4}
Cer(d18:1/18:0)	2.245	1.1667	8.93×10^{-4}

NSCLC: non-small cell lung cancer; fold-change values represent the ratio between NSCLC patients and healthy controls; values > 1 indicate higher abundance in NSCLC, whereas values < 1 indicate lower abundance.

The most strongly increased lEV-enriched fraction-associated lipid species in NSCLC included Cer(d18:2/16:0) and several triglycerides, notably TG(18:1_32:2), TG(16:1_34:0), and TG(16:1_32:1), whereas FA(14:0) and C14:1 showed decreased concentrations compared with controls. Overall, the top-ranked changes were dominated by ceramide and triglyceride species, consistent with the global NSCLC-associated lipid pattern observed in plasma-derived lEV-enriched fractions (Figure 3a).

To quantify within-cohort separation for individual analytes, exploratory ROC analyses were performed (Figure 3b). Cer(d18:2/16:0) showed the highest separation, with an AUC of 0.9726 (95% CI, 0.9415–1.000), followed by TG(18:1_32:2) (AUC 0.9452; 95% CI, 0.9015–0.9889), TG(16:1_34:0) (AUC 0.9110; 95% CI, 0.8556–0.9664), and TG(16:1_32:1) (AUC 0.8896; 95% CI, 0.8144–0.9647). Taken together, these lipid species showed strong within-cohort separation between NSCLC and control samples. To assess potential selection-

related optimism, exploratory internal validation was performed with repeated stratified five-fold cross-validation and bootstrap-based optimism correction, including repeated selection of the best-performing lipid within each resample. The mean cross-validated AUC was 0.9684, while the bootstrap optimism-corrected AUC was 0.9657, compared with an apparent AUC of 0.9726. These findings suggest that selection-related optimism was limited in this dataset, although independent validation remains necessary.

3.3. Distinct Lipids Show Exploratory Associations with Overall Survival

Cer(d18:2/16:0), TG(18:1_32:2), and TG(16:1_32:1) showed exploratory associations with overall survival in NSCLC. Kaplan–Meier analyses suggested shorter overall survival in patients with higher Cer(d18:2/16:0) levels, whereas higher TG(18:1_32:2) and TG(16:1_32:1) levels were associated with longer overall survival (Figure 4). Additional lipids showed non-significant associations with overall survival (Supplementary Figure S2). Patients with high TG(16:0_28:1) levels tended to have shorter overall survival than those with low levels (HR 1.753; 95% CI, 0.9316–3.299; $p = 0.0818$). A similar trend was observed for Cer(d18:1/24:1) (HR 1.921; 95% CI, 0.9521–3.876; $p = 0.0683$). By contrast, high TG(18:0_36:1) levels tended to be associated with longer overall survival (HR 0.6305; 95% CI, 0.3372–1.179; $p = 0.1485$). Because survival cutoffs were derived within the same dataset, these analyses were considered hypothesis-generating and require validation in independent cohorts.

3.4. Histological Subtype and PD-L1 Status Were Not Associated with Major Shifts in the Plasma-Derived lEV-Enriched Lipidome

To assess whether tumor PD-L1 expression was associated with changes in the lipidome of plasma-derived lEV-enriched fractions, NSCLC cases were stratified according to PD-L1 TPS using two clinically relevant thresholds (>50% vs. ≤50% and <1% vs. ≥1%). In the >50% vs. ≤50% comparison, fold-change filtering identified Cer(d18:2/18:1), PC ae C40:6, and PC aa C40:6 as increased species with a fold change >2 (Supplementary Figure S3a). In the <1% vs. ≥1% comparison, PC ae C40:6 showed a nominal signal in the volcano plot analysis (fold change 2.1695; raw $p = 0.0884$; Supplementary Figure S3b). However, these isolated findings were not supported by robust statistical evidence, as *t*-test-based results were uninformative and no multiple-testing-adjusted significance was observed. Overall, these data do not indicate a robust PD-L1-associated lipid signature in plasma-derived lEV-enriched fractions in this dataset.

Previous work has described subtype-specific extracellular vesicle-associated metabolic differences in cancer, although this was shown in breast cancer rather than NSCLC [28]. Since NSCLC comprises distinct histological subtypes, we next examined whether plasma-derived lEV-enriched lipid profiles differed between LUAD and LUSC.

When stratifying NSCLC by histology, LUAD samples showed separation from healthy controls in multivariate analysis of plasma-derived lEV-enriched lipid profiles (PCA; PC1 53.3%, PC2 13.2%; Figure 5a), indicating a LUAD-associated shift in the global lipidome of the enriched fraction. Differential abundance analysis revealed predominantly increased triglyceride and ceramide species in LUAD compared with controls, whereas selected fatty acids were decreased (Figure 5c). Hierarchical clustering of the differentially abundant lipid species supported cohort-level discrimination between LUAD and controls (Figure 5b).

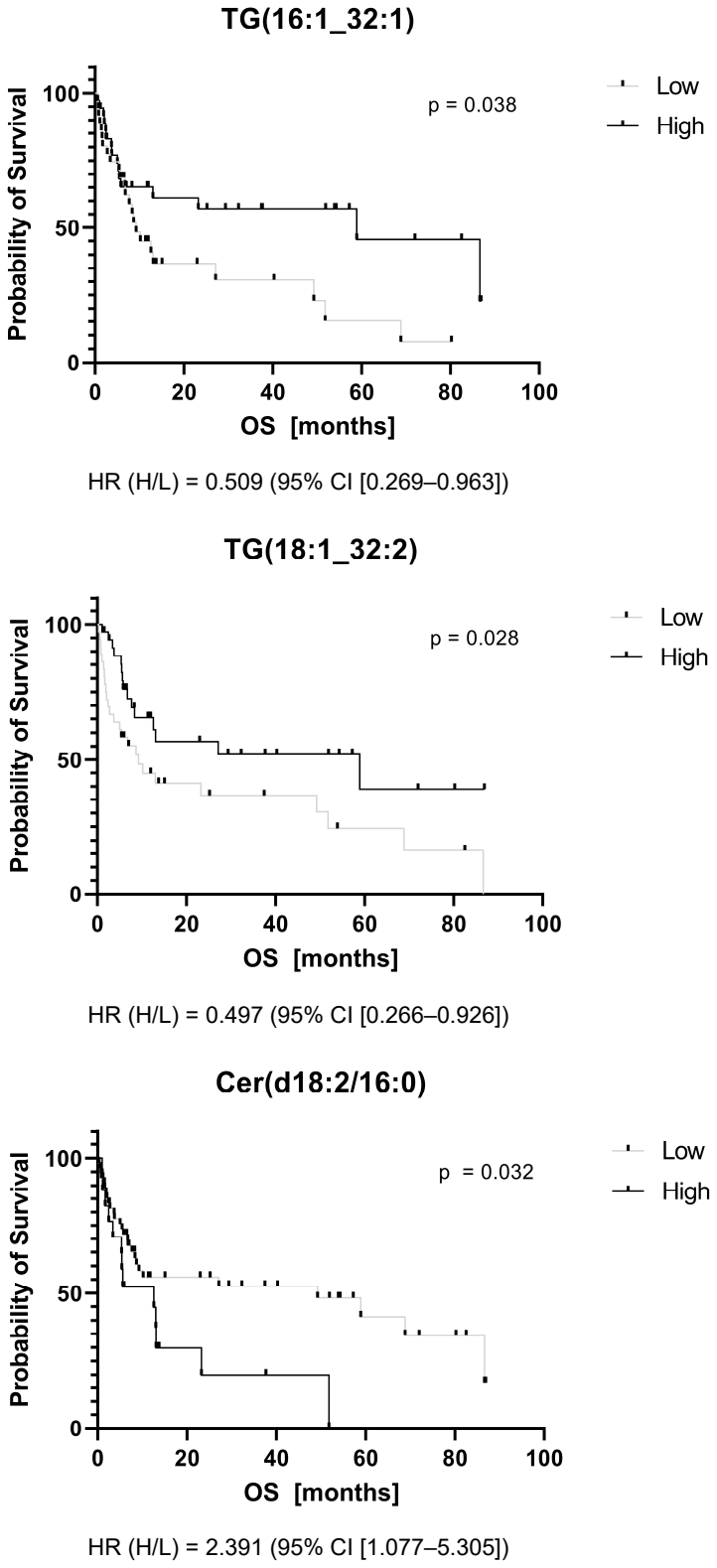

Figure 4. Exploratory associations between selected lipid species and overall survival in NSCLC. Kaplan–Meier curves showing overall survival of NSCLC patients stratified into high and low lipid groups for TG(16:1_32:1), TG(18:1_32:2), and Cer(d18:2/16:0) in plasma-derived large extracellular vesicle (lEV)-enriched fractions. Overall survival (OS) is shown in months. Groups were defined using data-driven cutoffs and compared using the log-rank test. Higher levels of TG(16:1_32:1) and TG(18:1_32:2) were associated with longer overall survival, whereas higher levels of Cer(d18:2/16:0) were associated with shorter overall survival. These analyses were exploratory and hypothesis-generating and require validation in independent cohorts. HR: hazard ratio.

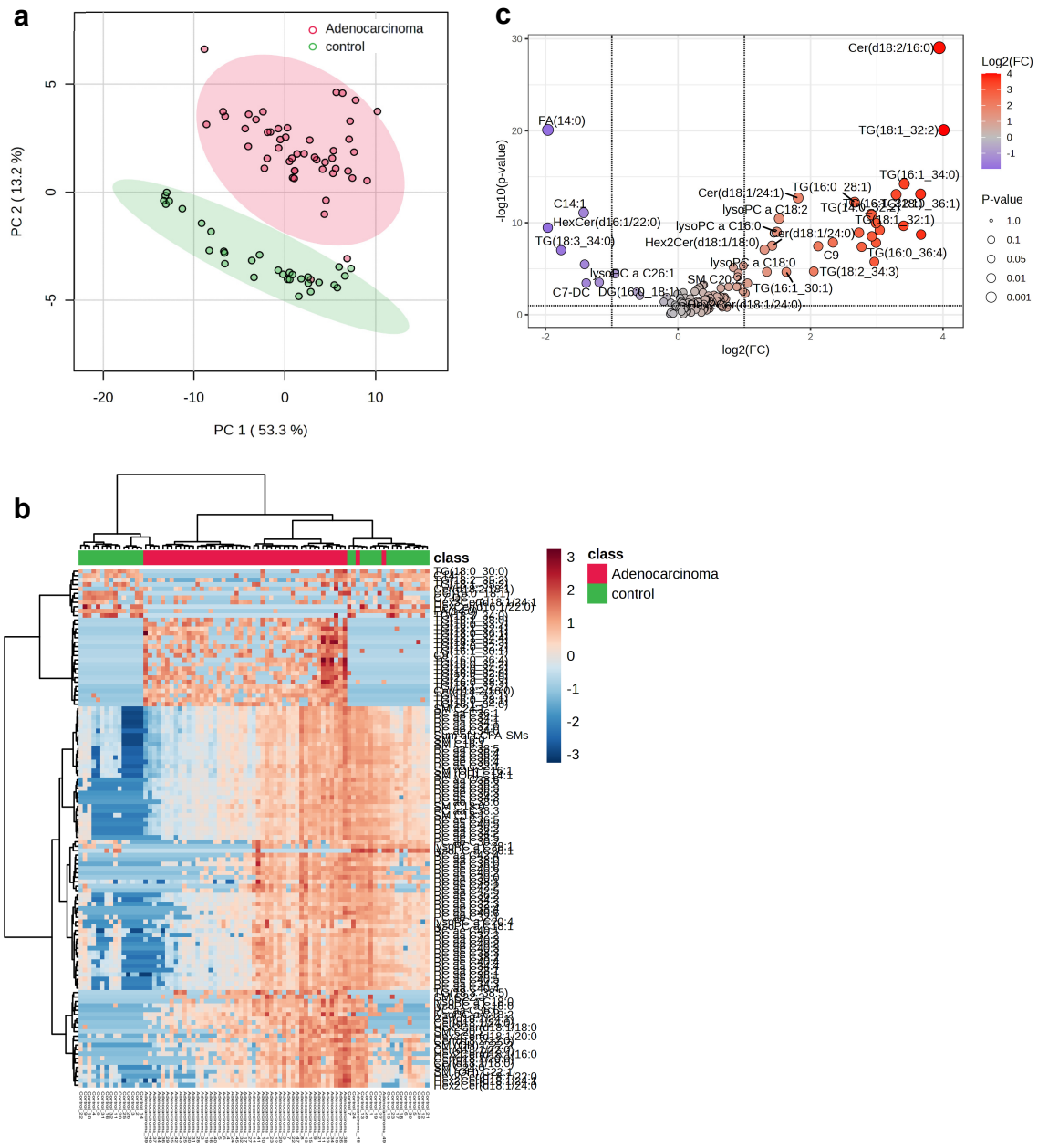

Figure 5. Lipid profiles of plasma-derived large extracellular vesicle (lEV)-enriched fractions in lung adenocarcinoma (LUAD) compared with healthy controls. (**a**) Principal component analysis of targeted lipidomic data from plasma-derived lEV-enriched fractions showing separation between LUAD samples and healthy controls. Each dot represents one sample. The first two principal components accounted for 53.3% and 13.2% of the total variance, respectively. Ellipses indicate the distribution of the respective sample groups. (**b**) Hierarchical clustering heatmap of lipid abundances in lung adenocarcinoma and control samples. Columns represent individual samples and rows represent lipid species. Values are shown as normalized relative abundances, with red indicating higher and blue indicating lower abundance. The upper annotation indicates sample class. (**c**) Volcano plot showing differential lipid abundance in LUAD ($n = 49$) compared with healthy controls ($n = 32$). The x-axis shows log2 fold change, and the y-axis shows −log10 raw p-value. Lipids with higher abundance in lung adenocarcinoma are shown on the right, whereas lipids with lower abundance are shown on the left. Dot color indicates log2 fold change, and dot size indicates p-value.

A comparable pattern was observed for LUSC. PCA demonstrated separation of LUSC from healthy controls based on plasma-derived lEV-enriched lipid profiles (PC1 55.1%, PC2 12.7%; Figure 6a). Differential abundance analysis was likewise dominated by increased

triglyceride and ceramide species, while selected fatty acids were reduced relative to controls (Figure 6c). Consistent with these findings, hierarchical clustering of the differentially abundant lipid species separated most LUSC samples from controls (Figure 6b).

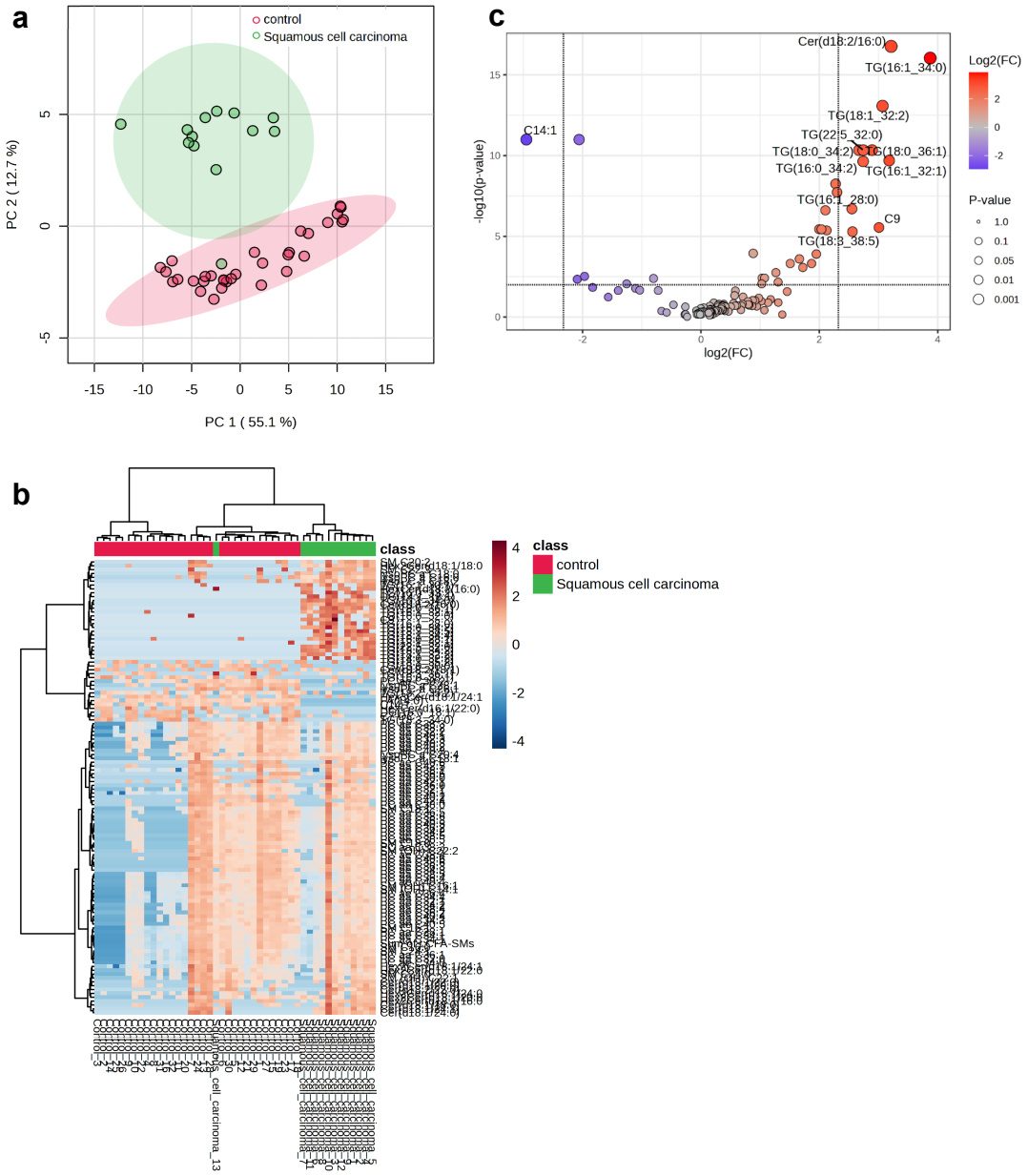

Figure 6. Lipid profiles of plasma-derived large extracellular vesicle (lEV)-enriched fractions in lung squamous cell carcinoma (LUSC) compared with healthy controls. (**a**) Principal component analysis of targeted lipidomic data from plasma-derived lEV-enriched fractions showing separation between LUSC samples and healthy controls. Each dot represents one sample. The first two principal components accounted for 55.1% and 12.7% of the total variance, respectively. Ellipses indicate the distribution of the respective sample groups. (**b**) Hierarchical clustering heatmap of lipid abundances in LUSC patients ($n = 13$) and controls ($n = 32$). Columns represent individual samples and rows represent lipid species. Values are shown as normalized relative abundances, with red indicating higher and blue indicating lower abundance. The upper annotation indicates sample class. (**c**) Volcano plot showing differential lipid abundance in LUSC compared with healthy controls. The x-axis shows log2 fold change, and the y-axis shows −log10 raw *p*-value. Lipids with higher abundance in LUSC are shown on the right, whereas lipids with lower abundance are shown on the left. Dot color indicates log2 fold change, and dot size indicates *p*-value.

3.5. NSCLC and SCLC Show Distinct Entity-Associated Lipid Profiles in Plasma-Derived lEV-Enriched Fractions

To further contextualize entity- and subtype-associated lipid alterations, we visualized the overlap of differential lipid species identified in the entity- and subtype-versus-control comparisons (NSCLC, SCLC, LUAD, and LUSC) using a Venn diagram (Figure 7d). Limited overlap was observed between SCLC-associated alterations and those identified in NSCLC and its histological subtypes, whereas substantial overlap was present among the NSCLC-related comparisons. No lipid species was shared across all four comparisons.

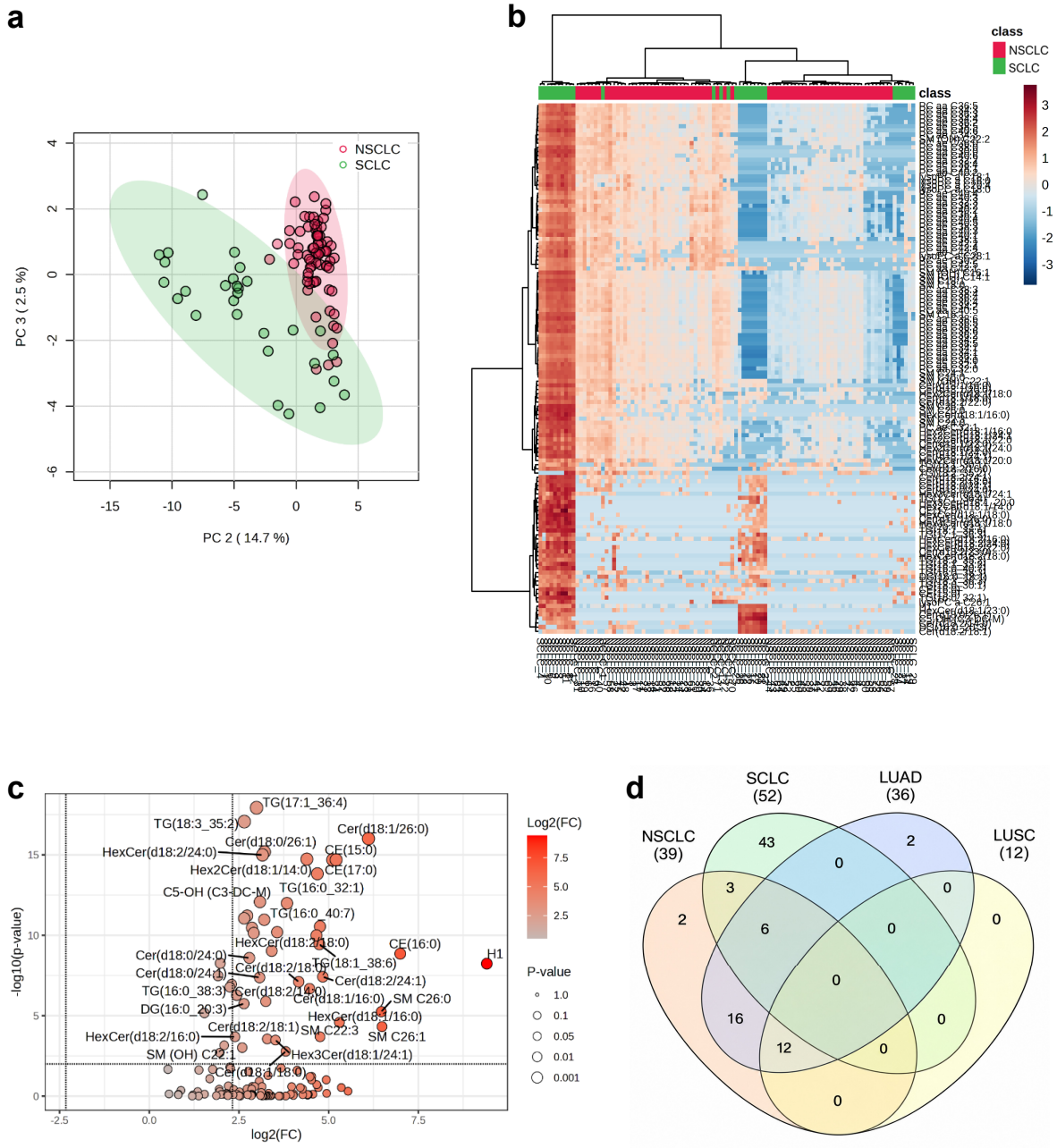

Figure 7. Entity-associated differences in plasma-derived large extracellular vesicle (lEV)-enriched lipid profiles across NSCLC, SCLC, and NSCLC histological subtypes. (**a**) Principal component analysis comparing lipid profiles of plasma-derived lEV-enriched fractions from NSCLC and SCLC samples. Each dot represents one sample. The displayed principal components accounted for 14.7% and 2.5% of the total variance, respectively. Ellipses indicate the distribution of the respective sample groups. (**b**) Hierarchical clustering heatmap of lipid abundances in NSCLC and SCLC samples. Columns

represent individual samples and rows represent lipid species. Values are shown as normalized relative abundances, with red indicating higher and blue indicating lower abundance. The upper annotation indicates tumor entity. (**c**) Volcano plot showing differential lipid abundance in SCLC ($n = 29$) compared with NSCLC ($n = 73$). The x-axis shows log2 fold change, and the y-axis shows −log10 raw *p*-value. Lipids with higher abundance in SCLC are shown on the right. Dot color indicates log2 fold change, and dot size indicates *p*-value. (**d**) Venn diagram showing the overlap of differentially abundant lipid species identified in the NSCLC-, SCLC-, lung adenocarcinoma (LUAD)-, and lung squamous cell carcinoma (LUSC)-versus-control comparisons. The overlap between SCLC-associated alterations and those identified in NSCLC and its histological subtypes was limited, whereas substantial overlap was observed among the NSCLC-related comparisons.

We then directly compared lipid profiles of plasma-derived lEV-enriched fractions from patients with NSCLC and SCLC. PCA and hierarchical clustering supported separation between NSCLC and SCLC samples (Figure 7a,b). Differential abundance analysis demonstrated pronounced between-entity differences, with multiple triglyceride and sphingolipid species showing higher abundance in SCLC relative to NSCLC, including long-chain ceramides and several cholesteryl esters (Figure 7c; Table 4). Together, these findings indicate that plasma-derived lEV-enriched fractions capture distinct lipidomic patterns in NSCLC and SCLC.

Table 4. Distinct metabolites of large extracellular vesicles in SCLC patients compared to NSCLC patients.

Metabolite	Fold Change	Log2 (Fold Change)	FDR-Adjusted *p*-Value
TG(17:1_36:4)	7.9488	2.9907	1.19×10^{-18}
TG(18:3_35:2)	6.2727	2.6491	8.60×10^{-18}
Cer(d18:1/26:0)	69.109	6.1108	9.81×10^{-17}
Cer(d18:0/26:1)	9.2644	3.2117	6.61×10^{-16}
HexCer(d18:2/24:0)	8.9103	3.1555	1.01×10^{-15}
Hex2Cer(d18:1/14:0)	21.011	4.3931	1.86×10^{-15}
CE(17:0)	37.013	5.21	2.04×10^{-15}
CE(15:0)	34.593	5.1124	2.04×10^{-15}
TG(16:0_32:1)	25.759	4.687	1.50×10^{-14}
C5-OH (C3-DC-M)	8.4891	3.0856	8.36×10^{-13}
TG(16:0_40:7)	14.307	3.8387	1.02×10^{-12}
Hex3Cer(d18:1_20:0)	6.6336	2.7298	6.08×10^{-12}
TG(18:1_33:2)	6.2508	2.644	8.83×10^{-12}
HexCer(d18:1/23:0)	9.2226	3.2052	1.08×10^{-11}
TG(20:4_32:1)	27.077	4.759	2.83×10^{-11}
Cer(d18:2/23:0)	7.2692	2.8618	3.41×10^{-11}
Hex3Cer(d18:1/18:0)	11.834	3.5649	6.38×10^{-11}
HexCer(d18:2/22:0)	7.5289	2.9124	7.25×10^{-11}
HexCer(d18:1/18:0)	25.296	4.6608	1.02×10^{-10}
TG(18:1_38:6)	26.741	4.741	3.59×10^{-10}
HexCer(d18:2/18:0)	10.656	3.4136	9.36×10^{-10}
CE(16:0)	127.7	6.9966	1.40×10^{-9}
Cer(d18:0/24:0)	6.9139	2.7895	2.56×10^{-9}
H1	680.05	9.4095	5.80×10^{-9}
Cer(d18:2/24:1)	28.605	4.8382	3.78×10^{-8}
Cer(d18:0/24:1)	8.43	3.0755	4.19×10^{-8}
Cer(d18:2/18:0)	17.947	4.1656	7.78×10^{-8}
Cer(d18:1/16:0)	22.13	4.4679	2.10×10^{-7}
TG(16:0_38:3)	5.4164	2.4373	5.36×10^{-7}
Cer(d18:2/14:0)	9.5006	3.248	1.29×10^{-6}
DG(16:0_20:3)	6.2363	2.6407	1.78×10^{-6}
SM C26:0	88.559	6.4686	5.61×10^{-6}
HexCer(d18:1/16:0)	39.426	5.3011	2.57×10^{-5}
SM C26:1	89.777	6.4883	4.75×10^{-5}
SM C22:3	27.141	4.7624	2.04×10^{-4}

Table 4. *Cont.*

Metabolite	Fold Change	Log2 (Fold Change)	FDR-Adjusted *p*-Value
HexCer(d18:2/16:0)	5.2398	2.3895	2.05×10^{-4}
Cer(d18:2/18:1)	9.7725	3.2887	2.78×10^{-4}
Hex3Cer(d18:1/24:1)	11.465	3.5192	3.26×10^{-4}
SM (OH) C22:1	6.0268	2.5914	9.60×10^{-4}

FDR: false discovery rate. NSCLC: non-small cell lung cancer. SCLC: small cell lung cancer. Fold change values represent the ratio between SCLC and NSCLC patients; values > 1 indicate higher abundance in SCLC.

Given the similar directionality of the dominant lipid alterations in both subtype-versus-control comparisons, we finally assessed whether LUAD and LUSC could be distinguished directly from each other. This analysis revealed broad overlap in global plasma-derived lEV-enriched lipid patterns and did not identify a consistent subtype-separating lipid signature (Supplementary Figure S4).

3.6. Exploratory Pathway Enrichment Implicates Sphingolipid-Related Signaling in NSCLC

Based on the set of differentially abundant lipid species identified in NSCLC versus controls, exploratory KEGG pathway enrichment analysis highlighted sphingolipid-related pathways among the top-ranked terms (Table 5). This observation is consistent with the lipid-class-level changes detected in NSCLC, particularly the prominence of ceramide-related alterations, and suggests that sphingolipid-associated lipid alterations are reflected in plasma-derived lEV-enriched fractions.

Table 5. Pathways identified by pathway enrichment analysis.

Comparison	Pathway Name	Converted Lipids	*p*-Value	Benjamini Correction
NSCLC vs. control	Sphingolipid signaling pathway	C12126, C00195	0.000743892	0.005951135
	Sphingolipid metabolism	C00195, C12126	0.004273911	0.017095642
	AGE-RAGE signaling pathway in diabetic complications	C00195	0.011152339	0.022221452
	Neurotrophin signaling pathway	C00195	0.016697279	0.022221452
	Adipocytokine signaling pathway	C00195	0.016697279	0.022221452
	Necroptosis	C00195	0.022221452	0.022221452
	Leishmaniasis	C00195	0.022221452	0.022221452
	Insulin resistance	C00195	0.022221452	0.022221452
NSCLC vs. SCLC	Sphingolipid signaling pathway	C12126, C00195	0.003622918	0.05072085
	Sphingolipid metabolism	C00195, C12126	0.019892185	0.077123349
	AGE-RAGE signaling pathway in diabetic complications	C00195	0.022242141	0.077123349
	Neurotrophin signaling pathway	C00195	0.03320765	0.077123349
	Adipocytokine signaling pathway	C00195	0.03320765	0.077123349
	Necroptosis	C00195	0.044070485	0.077123349
	Insulin resistance	C00195	0.044070485	0.077123349
	Leishmaniasis	C00195	0.044070485	0.077123349

NSCLC: non-small cell lung cancer. SCLC: small cell lung cancer. KEGG identifiers may represent multiple molecular lipid species within the same lipid class. Therefore, the number of mapped identifiers does not necessarily correspond to the number of experimentally altered lipid species. Pathway enrichment was exploratory and does not indicate functional pathway activation or suppression.

As sphingolipids are involved in membrane architecture, signal transduction, and cancer-associated cellular adaptation [35], these results may point to biologically meaningful

disease-associated remodeling. In the NSCLC versus SCLC comparison, pathway analysis suggested similar top-ranked pathways; however, these did not remain significant after multiple-testing correction. Thus, while the overall pattern was comparable, the between-entity pathway results should be interpreted with caution.

4. Discussion

NSCLC remains a leading cause of cancer mortality, and clinically robust blood-based biomarkers for early detection, biologic stratification, and outcome prediction remain limited. While liquid biopsy approaches such as circulating tumor DNA provide actionable genomic information, they do not directly capture downstream metabolic phenotypes that may reflect tumor biology and tumor–host interactions. In this context, circulating extracellular vesicles represent a complementary analyte class, as they transport bioactive cargo and may integrate features of both the tumor and the systemic response [1,36–39].

In this exploratory study, we applied targeted mass spectrometry to characterize the lipid cargo of plasma-derived lEV-enriched fractions in NSCLC and compared the resulting lipid profiles with healthy controls and an SCLC cohort. The objective was not to define a clinical test, but to establish a descriptive reference of lEV lipid alterations at the cohort level and to generate hypotheses for future validation and mechanistic work. Building on our previous studies of circulating lEV-enriched fractions in breast cancer [28] and SCLC [27], the present work extends targeted lipidomic profiling to NSCLC and directly compares lipid signatures between NSCLC and SCLC within a common analytical workflow. This approach provides new insights into entity-associated lipid alterations in plasma-derived lEV-enriched fractions, an area that remains insufficiently investigated.

Three main findings emerge. First, NSCLC patients displayed a distinct lEV lipid pattern compared with controls, supported by multivariate separation and a defined set of differentially abundant species. The alterations were dominated by changes in selected ceramide and triglyceride species, including increased Cer(d18:2/16:0) and several triglycerides, alongside reduced FA(14:0) and C14:1. Among our top-ranked lipid species, the strongest overlap with prior reports at the molecular-species level was observed for Cer(d18:2/16:0), which was also identified in NSCLC tissue lipidomics, and for Cer(d18:1/24:1), which has previously been implicated in circulating lipid studies of lung cancer [40–42]. Notably, Cer(d18:2/16:0) was reported to be decreased in NSCLC tissue [42], contrasting with its increased abundance in our plasma-derived lEV-enriched fractions. By contrast, for most triglyceride species and for FA(14:0), C14:1, and HexCer(d16:1/22:0), the available literature more strongly supports concordant class-level alterations—particularly triglyceride enrichment, free fatty acid depletion, and glycosphingolipid remodeling—than exact recurrence of the same molecular species [41,43–45]. Consistent with our findings, Fan et al. identified altered lipid profiles in plasma-derived exosomes from NSCLC patients [46]. Similarly, Smolarz et al., using a Biocrates-based approach, reported increased Cer(42:1), TG(54:2), and CE(19:2), alongside decreased PC(38:6), in serum-derived sEVs from lung cancer patients compared with healthy controls [47]. Yang et al. additionally demonstrated altered metabolomic profiles in urinary EVs from lung cancer patients [48]. However, direct comparisons remain limited by differences in biological fluids, analytical methods, and EV populations, particularly because previous studies predominantly investigated sEVs or exosomes rather than lEV-enriched fractions [46–48]. The increased abundance of several triglyceride species may reflect cancer-associated alterations in lipid metabolism, including changes in lipid storage and mobilization. Although the absence of detectable APOA1 in our Western blot analysis suggests limited co-enrichment of APOA1-containing lipoproteins, contributions from other lipoprotein-associated particles cannot be entirely

excluded. Therefore, the underlying mechanisms responsible for the increased triglyceride abundance remain to be elucidated.

Second, the lEV lipidome differed markedly between NSCLC and SCLC within this dataset, with limited overlap of altered metabolites. Given that plasma EV preparations represent a composite of vesicles from multiple cellular sources [10,13], this entity-associated divergence is notable and supports the concept that tumor-linked biology can contribute measurably to circulating lEV cargo despite biological heterogeneity. Third, hypothesis-generating survival analyses suggested that variation in selected plasma-derived lEV lipids may relate to overall survival. This observation is in line with our recent SCLC study, in which higher concentrations of several lEV-associated lipids were likewise linked to shorter survival [27]. It is broadly consistent with prior blood-based metabolomic and lipidomic studies in NSCLC that associated lipid alterations with clinical outcome or treatment response [49–51]. The observed lipid shifts align with the broader framework of cancer-associated metabolic reprogramming [52–54]. Malignant cells reprogram lipid metabolism to support membrane biogenesis, energy production, and cellular signaling [55]. Within the tumor microenvironment, these adaptations also affect interactions between malignant, stromal, and immune cells and can promote tumor progression and immune suppression [56].

Exploratory KEGG pathway analysis identified sphingolipid-related pathways among the top-ranked terms in NSCLC versus controls (Table 5). A similar signal was observed in our recent SCLC lEV study, in which pathway analysis also implicated sphingolipid signaling [27]. The recurrence of sphingolipid-related pathways in both lung cancer cohorts may indicate a shared contribution of sphingolipid alterations to their circulating lEV-enriched lipid profiles. In contrast, our previous analysis of blood-derived lEV-enriched fractions in breast cancer predominantly identified glycerophospholipid and ether lipid metabolism [28], suggesting that the pathways highlighted by such analyses may vary across cancer entities and analytical approaches. The recurrence of sphingolipid-related findings in both lung cancer cohorts is biologically notable because sphingolipid signaling, including ceramide biology, has been implicated in tumor progression, stress adaptation, and treatment response [35]. It may also point to potentially targetable signaling nodes rather than merely descriptive pathway labels, although the present data remain strictly hypothesis-generating. At the same time, pathway enrichment results require cautious interpretation because KEGG mapping depends on successful identifier conversion and captures only the subset of altered lipids that can be assigned to pathway annotations [34,57]. Importantly, multiple distinct lipid species, such as ceramides with different fatty acyl compositions, may be mapped to the same generic KEGG identifier, resulting in a loss of molecular information. In our analysis, sphingolipid-related pathways were represented by only two mapped KEGG identifiers, while several other pathway terms were associated with a single identifier; consequently, these results cannot establish functional pathway activation or suppression. Apparent enrichment may therefore be driven by a limited number of mapped identifiers rather than by a comprehensive pathway-level shift. Accordingly, these pathway results should be viewed as a structured framework for prioritizing sphingolipid-centered follow-up studies in vesicle fractions rather than as direct evidence for immediate therapeutic actionability. Thus, the prominence of sphingolipid-related pathways may reflect both the observed alterations in ceramide species and the analytical coverage and pathway mapping of the targeted lipidomics platform, rather than demonstrating that other lipid metabolic pathways are unaffected.

A key methodological consideration is that differential centrifugation enriches a vesicle fraction but does not selectively isolate tumor-derived vesicles and may co-enrich platelet-derived vesicles and other large particles [10,13]. Consequently, the detected lipid patterns

likely represent an integrated signal from tumor and host compartments rather than a tumor-exclusive readout. This composite nature may also contribute to the absence of clear lipid differences in PD-L1-stratified analyses and to the largely overlapping global lipid patterns between LUAD and LUSC in this cohort. Within the limits of sample size and cohort composition, these results suggest that PD-L1 strata and NSCLC histology were not dominant drivers of the lEV lipidome in this dataset, although subtle effects cannot be excluded.

Limitations

Several limitations deserve emphasis. This single-center observational study predominantly reflects advanced and/or metastatic disease, limiting generalizability to early-stage NSCLC. Controls were younger than patients, and residual confounding from age-related lipid metabolism cannot be excluded. The substantial age difference between NSCLC patients (median 62.4 years) and healthy controls (median 43 years) may therefore have contributed to the observed lipidomic differences. In addition, information on smoking history, metabolic comorbidities, and lipid-lowering medication was not systematically available for all participants, particularly because some healthy controls were recruited from blood donors for whom only age and sex were available. Consequently, a comprehensive multivariable analysis accounting for these potential confounders was not feasible. Although the study included both male and female participants, potential effects of age, sex, smoking, metabolic status, and treatment exposure on the observed lipid profiles cannot be fully disentangled from disease-associated differences. Furthermore, routine laboratory parameters were not consistently available at the time of blood sampling across the extended recruitment period, precluding a systematic assessment of potential associations between laboratory findings and lipid profiles. Protein-based normalization was performed throughout the workflow and followed a previously validated lEV-enrichment protocol. The main limitation is therefore not the absence of normalization, but that the analyzed fraction represents an enriched mixed lEV population rather than a purified tumor-specific vesicle subset. EV isolation and characterization are further complicated by overlapping particle size distributions, morphological heterogeneity, and variable molecular composition [10,13]. In our study, NTA was restricted to five healthy control preparations and could not establish the size distribution of EVs across the entire cohort. Similarly, Western blot analysis was performed on three representative patient-derived preparations to characterize the enrichment procedure rather than to assess individual sample composition. Although standardized processing and protein-based normalization were applied across all cohorts, systematic cohort-wide particle characterization was not performed, and potential differences in the composition of the enriched fractions cannot be excluded. Moreover, electron microscopy was not performed to assess vesicle morphology, and differential centrifugation cannot completely exclude co-enrichment of lipoproteins and other extracellular particles, which may influence the detected lipid profiles. Therefore, we deliberately refer to the analyzed material as a plasma-derived lEV-enriched fraction rather than a purified lEV population, acknowledging the potential contribution of co-enriched extracellular particles to the detected lipid profiles. Finally, multiple comparisons and data-driven procedures (including exploratory ROC metrics and cutpoint-based survival visualization) were conducted within the same dataset and may be subject to optimism bias. Independent validation, prospective sampling, and multivariable modeling will be essential to assess reproducibility and translational relevance.

In summary, targeted lipidomic profiling of plasma-derived lEVs identified a distinct NSCLC-associated lipid pattern and largely non-overlapping alterations between NSCLC and SCLC within this cohort. These findings provide a descriptive reference for lEV lipid

changes in NSCLC and define testable hypotheses for future mechanistic and biomarker-oriented studies.

5. Conclusions

Plasma-derived lEV-enriched fractions from NSCLC patients exhibit a distinct lipid profile compared with healthy controls, dominated by alterations in ceramide and triglyceride species. The largely non-overlapping lipid alterations observed between NSCLC and SCLC support entity-associated lipid profiles in these fractions. Independent multicenter validation with standardized EV characterization and clinically relevant comparator cohorts will be required to determine robustness and potential clinical utility.

Supplementary Materials: The following supporting information can be downloaded at: https://www.mdpi.com/article/10.3390/cancers18233823/s1, Figure S1: Schematic overview of the study design and analytical workflow; Figure S2: Exploratory associations between additional lipid species and overall survival in NSCLC; Figure S3: PD-L1-stratified comparisons of plasma-derived large extracellular vesicle-enriched lipid profiles in NSCLC; Figure S4: Additional comparisons of plasma-derived large extracellular vesicle-enriched lipid profiles between lung adenocarcinoma and lung squamous cell carcinoma; Figure S5: Original Western blot images and corresponding Ponceau S staining used for the characterization of plasma-derived large extracellular vesicle-enriched fractions shown in Figure 1b.

Author Contributions: Conceptualization, S.N., M.S. and J.B.; methodology, S.N., S.S., M.S. and J.B.; software, S.S., S.N. and J.B.; validation, S.N., S.S., A.C.A. and J.B.; formal analysis, S.N., A.C.A., A.v.H.-E. and J.B.; investigation, S.N. and J.B.; resources, J.B.; data curation, S.N.; writing—original draft preparation, S.N. and J.B.; writing—review and editing, all authors; visualization, S.N., A.C.A. and J.B.; supervision, J.B.; project administration, J.B.; funding acquisition, J.B. All authors have read and agreed to the published version of the manuscript.

Funding: This research was funded by the Else Kröner-Fresenius Foundation and Stiftung Gerdes.

Institutional Review Board Statement: The study was approved by the local Ethics Committee of the University Medical Center Göttingen (approval no. 3/2/14; approval date: 17 March 2014) and was conducted in accordance with the Declaration of Helsinki. Written informed consent was obtained from all participants prior to inclusion.

Informed Consent Statement: Informed consent was obtained from all subjects involved in the study.

Data Availability Statement: The data supporting the findings of this study are not publicly available due to privacy and ethical restrictions associated with sensitive patient health information. Data may be made available by the corresponding author upon reasonable request, subject to applicable data protection regulations and ethical approval requirements.

Acknowledgments: The authors would like to sincerely thank all patients who participated in this study for their valuable contribution. During the preparation of this manuscript, the authors used ChatGPT (OpenAI, GPT-6) for the purposes of language editing, improving clarity, and refining the scientific wording of the text. The authors have reviewed and edited the output and take full responsibility for the content of this publication.

Conflicts of Interest: The authors declare no conflicts of interest. The funding foundations provided financial support following the evaluation and approval of the research grant applications. The funders had no role in the design of the study; in the collection, analyses, or interpretation of data; in the writing of the manuscript; or in the decision to publish the results.

Abbreviations

Abbreviation	Full term
ACTININ-4	Alpha-actinin-4
AGE	Advanced glycation end products
APOA1	Apolipoprotein A-I
AUC	Area under the curve
CE	Cholesteryl ester
Cer	Ceramide
CI	Confidence interval
DG	Diacylglycerol
EDTA	Ethylenediaminetetraacetic acid
EV	Extracellular vesicle
FA	Fatty acid
FDR	False discovery rate
FIA-MS/MS	Flow injection analysis tandem mass spectrometry
Hex2Cer	Dihexosylceramide
Hex3Cer	Trihexosylceramide
HexCer	Hexosylceramide
HR	Hazard ratio
KEGG	Kyoto Encyclopedia of Genes and Genomes
LC-MS/MS	Liquid chromatography tandem mass spectrometry
lEV	Large extracellular vesicle
LIPEA	Lipid Pathway Enrichment Analysis
LUAD	Lung adenocarcinoma
LUSC	Lung squamous cell carcinoma
lysoPC	Lysophosphatidylcholine
MISEV	Minimal Information for Studies of Extracellular Vesicles
MRM	Multiple reaction monitoring
MxP	Metabolomics Profiling
NSCLC	Non-small cell lung cancer
NTA	Nanoparticle tracking analysis
OS	Overall survival
PBS	Phosphate-buffered saline
PC	Principal component/Phosphatidylcholine
PC aa	Diacylphosphatidylcholine
PC ae	Acyl-alkylphosphatidylcholine
PCA	Principal component analysis
PD-1	Programmed cell death protein 1
PD-L1	Programmed death-ligand 1
RAGE	Receptor for advanced glycation end products
RGAP1	Rho GTPase-activating protein 1
ROC	Receiver operating characteristic
SCLC	Small cell lung cancer
SDS-PAGE	Sodium dodecyl sulfate polyacrylamide gel electrophoresis
SM	Sphingomyelin
TBST	Tris-buffered saline with Tween-20
TTF-1	Thyroid transcription factor 1
TG	Triglyceride
TPS	Tumor proportion score

References

1. Sung, H.; Filho, A.M.; Laversanne, M.; Ferlay, J.; Siegel, R.L.; Soerjomataram, I.; Jemal, A.; Bray, F. Global cancer statistics 2024: GLOBOCAN estimates of incidence and mortality worldwide for 34 cancers in 186 countries. *CA Cancer J. Clin.* **2026**, *76*, e70090. [CrossRef] [PubMed]
2. World Health Organization (WHO). Lung Cancer. Fact Sheet. Available online: https://www.who.int/news-room/fact-sheets/detail/lung-cancer (accessed on 27 January 2026).
3. Robert Koch Institute (RKI); Zentrum für Krebsregisterdaten (ZfKD). Lungenkrebs. Available online: https://www.krebsdaten.de/Krebs/DE/Content/Krebsarten/Lungenkrebs/lungenkrebs_node.html (accessed on 27 January 2026).
4. Sharma, P.; Hu-Lieskovan, S.; Wargo, J.A.; Ribas, A. Primary, Adaptive and Acquired Resistance to Cancer Immunotherapy. *Cell* **2017**, *168*, 707–723. [CrossRef] [PubMed]

5. Sharma, P.; Goswami, S.; Raychaudhuri, D.; Siddiqui, B.A.; Singh, P.; Nagarajan, A.; Liu, J.; Subudhi, S.K.; Poon, C.; Gant, K.L.; et al. Immune checkpoint therapy-current perspectives and future directions. *Cell* **2023**, *186*, 1652–1669. [CrossRef] [PubMed]
6. Ning, J.; Ge, T.; Jiang, M.; Jia, K.; Wang, L.; Li, W.; Chen, B.; Liu, Y.; Wang, H.; Zhao, S.; et al. Early diagnosis of lung cancer: Which is the optimal choice? *Aging* **2021**, *13*, 6214–6227. [CrossRef] [PubMed]
7. Revel, M.-P.; Biederer, J.; Nair, A.; Silva, M.; Jacobs, C.; Snoeckx, A.; Prokop, M.; Prosch, H.; Parkar, A.P.; Frauenfelder, T.; et al. ESR Essentials: Lung cancer screening with low-dose CT—Practice recommendations by the European Society of Thoracic Imaging. *Eur. Radiol.* **2026**, *36*, 2064–2073. [CrossRef] [PubMed]
8. Huang, W.; Zhao, M.; Li, L.; Chen, Q.; Yang, M.; Zhou, C.; Qi, M.; Wang, Y.; Luo, L.; Liang, W.; et al. Extracellular vesicle biomarkers: Current status and future perspectives as novel tools in liquid biopsy. *Front. Immunol.* **2026**, *17*, 1853671. [CrossRef] [PubMed]
9. Witwer, K.W.; Buzás, E.I.; Bemis, L.T.; Bora, A.; Lässer, C.; Lötvall, J.; Nolte-'t Hoen, E.N.; Piper, M.G.; Sivaraman, S.; Skog, J.; et al. Standardization of sample collection, isolation and analysis methods in extracellular vesicle research. *J. Extracell. Vesicles* **2013**, *2*, 20360. [CrossRef] [PubMed]
10. Théry, C.; Witwer, K.W.; Aikawa, E.; Alcaraz, M.J.; Anderson, J.D.; Andriantsitohaina, R.; Antoniou, A.; Arab, T.; Archer, F.; Atkin-Smith, G.K.; et al. Minimal information for studies of extracellular vesicles 2018 (MISEV2018): A position statement of the International Society for Extracellular Vesicles and update of the MISEV2014 guidelines. *J. Extracell. Vesicles* **2018**, *7*, 1535750. [CrossRef] [PubMed]
11. Raposo, G.; Stoorvogel, W. Extracellular vesicles: Exosomes, microvesicles, and friends. *J. Cell Biol.* **2013**, *200*, 373–383. [CrossRef] [PubMed]
12. van Niel, G.; D'Angelo, G.; Raposo, G. Shedding light on the cell biology of extracellular vesicles. *Nat. Rev. Mol. Cell Biol.* **2018**, *19*, 213–228. [CrossRef] [PubMed]
13. Welsh, J.A.; Goberdhan, D.C.I.; O'Driscoll, L.; Buzas, E.I.; Blenkiron, C.; Bussolati, B.; Cai, H.; Di Vizio, D.; Driedonks, T.A.P.; Erdbrügger, U.; et al. Minimal information for studies of extracellular vesicles (MISEV2023): From basic to advanced approaches. *J. Extracell. Vesicles* **2024**, *13*, e12404. Correction in *J. Extracell. Vesicles* **2024**, *13*, e12451. https://doi.org/10.1002/jev2.12451. [CrossRef] [PubMed]
14. Cocucci, E.; Meldolesi, J. Ectosomes and exosomes: Shedding the confusion between extracellular vesicles. *Trends Cell Biol.* **2015**, *25*, 364–372. [CrossRef] [PubMed]
15. Budayr, O.M.; Miller, B.C.; Nguyen, J. Harnessing extracellular vesicle-mediated crosstalk between T cells and cancer cells for therapeutic applications. *J. Control. Release* **2025**, *378*, 266–280. [CrossRef] [PubMed]
16. Liu, Q.; Xiang, Y.; Yuan, S.; Xie, W.; Li, C.; Hu, Z.; Wu, N.; Wu, L.; Yu, Z.; Bai, L.; et al. Plasma exosome levels in non-small-cell lung cancer: Correlation with clinicopathological features and prognostic implications. *Cancer Biomark.* **2018**, *22*, 267–274. [CrossRef] [PubMed]
17. Coumans, F.A.W.; Brisson, A.R.; Buzas, E.I.; Dignat-George, F.; Drees, E.E.E.; El-Andaloussi, S.; Emanueli, C.; Gasecka, A.; Hendrix, A.; Hill, A.F.; et al. Methodological Guidelines to Study Extracellular Vesicles. *Circ. Res.* **2017**, *120*, 1632–1648. [CrossRef] [PubMed]
18. Lucien, F.; Gustafson, D.; Lenassi, M.; Li, B.; Teske, J.J.; Boilard, E.; von Hohenberg, K.C.; Falcón-Perez, J.M.; Gualerzi, A.; Reale, A.; et al. MIBlood-EV: Minimal information to enhance the quality and reproducibility of blood extracellular vesicle research. *J. Extracell. Vesicles* **2023**, *12*, e12385. [CrossRef] [PubMed]
19. Newman, L.; Rowland, A. Detection and Isolation of Tissue-Specific Extracellular Vesicles from the Blood. *J. Extracell. Biol.* **2025**, *4*, e70059. [CrossRef] [PubMed]
20. Del Re, M.; Marconcini, R.; Pasquini, G.; Rofi, E.; Vivaldi, C.; Bloise, F.; Restante, G.; Arrigoni, E.; Caparello, C.; Bianco, M.G.; et al. PD-L1 mRNA expression in plasma-derived exosomes is associated with response to anti-PD-1 antibodies in melanoma and NSCLC. *Br. J. Cancer* **2018**, *118*, 820–824. [CrossRef] [PubMed]
21. Wang, Y.; Niu, X.; Cheng, Y.; Zhang, Y.; Xia, L.; Xia, W.; Lu, S. Exosomal PD-L1 predicts response with immunotherapy in NSCLC patients. *Clin. Exp. Immunol.* **2022**, *208*, 316–322. [CrossRef] [PubMed]
22. Hur, J.Y.; Kim, H.J.; Lee, J.S.; Choi, C.M.; Lee, J.C.; Jung, M.K.; Pack, C.G.; Lee, K.Y. Extracellular vesicle-derived DNA for performing EGFR genotyping of NSCLC patients. *Mol. Cancer* **2018**, *17*, 15. [CrossRef] [PubMed]
23. Vasu, S.; Johnson, V.; Archana, M.; Reddy, K.A.; Sukumar, U.K. Circulating Extracellular Vesicles as Promising Biomarkers for Precession Diagnostics: A Perspective on Lung Cancer. *ACS Biomater. Sci. Eng.* **2025**, *11*, 95–134. [CrossRef] [PubMed]
24. Carreca, A.P.; Tinnirello, R.; Miceli, V.; Galvano, A.; Gristina, V.; Incorvaia, L.; Pampalone, M.; Taverna, S.; Iannolo, G. Extracellular Vesicles in Lung Cancer: Implementation in Diagnosis and Therapeutic Perspectives. *Cancers* **2024**, *16*, 1967. [CrossRef] [PubMed]
25. Soupir, A.C.; Tian, Y.; Stewart, P.A.; Nunez-Lopez, Y.O.; Manley, B.J.; Pellini, B.; Bloomer, A.M.; Zhang, J.; Mo, Q.; Marchion, D.C.; et al. Detectable Lipidomes and Metabolomes by Different Plasma Exosome Isolation Methods in Healthy Controls and Patients with Advanced Prostate and Lung Cancer. *Int. J. Mol. Sci.* **2023**, *24*, 1830. [CrossRef] [PubMed]

26. Mayhew, M.; Megram, O.; Roshan, S.; Smith, M.J.; White, S.J.; Wilson, P.B.; Hunt, J.A.; De Girolamo, L.; James, V.; Hunter, E. Evidence of cancer: A systematic review of metabolomics in extracellular vesicles for cancer biomarker detection. *Metabolomics* **2026**, *22*, 13. [CrossRef] [PubMed]
27. Naser, S.; Schulz, M.; Schuchardt, S.; Hammerstein-Equord, A.V.; Büntzel, J. Metabolomic Profiling of Large Extracellular Vesicles in Patients Suffering from Small Cell Lung Cancer. *Anticancer Res.* **2024**, *44*, 4729–4735. [CrossRef] [PubMed]
28. Buentzel, J.; Klemp, H.G.; Kraetzner, R.; Schulz, M.; Dihazi, G.H.; Streit, F.; Bleckmann, A.; Menck, K.; Wlochowitz, D.; Binder, C. Metabolomic Profiling of Blood-Derived Microvesicles in Breast Cancer Patients. *Int. J. Mol. Sci.* **2021**, *22*, 13540. [CrossRef] [PubMed]
29. Pang, Z.; Lu, Y.; Zhou, G.; Hui, F.; Xu, L.; Viau, C.; Spigelman, A.F.; MacDonald, P.E.; Wishart, D.S.; Li, S.; et al. MetaboAnalyst 6.0: Towards a unified platform for metabolomics data processing, analysis and interpretation. *Nucleic Acids Res.* **2024**, *52*, W398–W406. [CrossRef] [PubMed]
30. Benjamini, Y.; Hochberg, Y. Controlling the False Discovery Rate: A Practical and Powerful Approach to Multiple Testing. *J. R. Stat. Soc. Ser. B Methodol.* **1995**, *57*, 289–300. [CrossRef]
31. Hanley, J.A.; McNeil, B.J. The meaning and use of the area under a receiver operating characteristic (ROC) curve. *Radiology* **1982**, *143*, 29–36. [CrossRef] [PubMed]
32. Camp, R.L.; Dolled-Filhart, M.; Rimm, D.L. X-tile: A new bio-informatics tool for biomarker assessment and outcome-based cut-point optimization. *Clin. Cancer Res.* **2004**, *10*, 7252–7259. [CrossRef] [PubMed]
33. Acevedo, A.; Durán, C.; Ciucci, S.; Gerl, M.; Cannistraci, C.V. LIPEA: Lipid Pathway Enrichment Analysis. *bioRxiv* **2018**. [CrossRef]
34. Kanehisa, M.; Goto, S. KEGG: Kyoto Encyclopedia of Genes and Genomes. *Nucleic Acids Res.* **2000**, *28*, 27–30. [CrossRef] [PubMed]
35. Ogretmen, B. Sphingolipid metabolism in cancer signalling and therapy. *Nat. Rev. Cancer* **2018**, *18*, 33–50. [CrossRef] [PubMed]
36. Irmer, B.; Chandrabalan, S.; Maas, L.; Bleckmann, A.; Menck, K. Extracellular Vesicles in Liquid Biopsies as Biomarkers for Solid Tumors. *Cancers* **2023**, *15*, 1307. [CrossRef] [PubMed]
37. Bhalla, S.; Yi, S.; Gerber, D.E. Emerging Strategies in Lung Cancer Screening: Blood and Beyond. *Clin. Chem.* **2024**, *70*, 60–67. [CrossRef] [PubMed]
38. Rayamajhi, S.; Sipes, J.; Tetlow, A.L.; Saha, S.; Bansal, A.; Godwin, A.K. Extracellular Vesicles as Liquid Biopsy Biomarkers across the Cancer Journey: From Early Detection to Recurrence. *Clin. Chem.* **2024**, *70*, 206–219. [CrossRef] [PubMed]
39. Makar, K.; Wróbel, A.; Antczak, A.; Tworek, D. Clinical Utility of ctDNA Analysis in Lung Cancer—A Review. *Adv. Respir. Med.* **2025**, *93*, 17. [CrossRef] [PubMed]
40. Yang, D.; Yang, X.; Li, Y.; Zhao, P.; Fu, R.; Ren, T.; Hu, P.; Wu, Y.; Yang, H.; Guo, N. Clinical significance of circulating tumor cells and metabolic signatures in lung cancer after surgical removal. *J. Transl. Med.* **2020**, *18*, 243. [CrossRef] [PubMed]
41. Hwang, B.Y.; Seo, J.W.; Muftuoglu, C.; Mert, U.; Guldaval, F.; Asadi, M.; Karakus, H.S.; Goksel, T.; Veral, A.; Caner, A.; et al. Salivary Lipids of Patients with Non-Small Cell Lung Cancer Show Perturbation with Respect to Plasma. *Int. J. Mol. Sci.* **2023**, *24*, 14264. [CrossRef] [PubMed]
42. Zhang, J.; Zang, X.; Jiao, P.; Wu, J.; Meng, W.; Zhao, L.; Lv, Z. Alterations of Ceramides, Acylcarnitines, GlyceroLPLs, and Amines in NSCLC Tissues. *J. Proteome Res.* **2024**, *23*, 4343–4358. [CrossRef] [PubMed]
43. Fan, Y.; Noreldeen, H.A.A.; You, L.; Liu, X.; Pan, X.; Hou, Z.; Li, Q.; Li, X.; Xu, G. Lipid alterations and subtyping maker discovery of lung cancer based on nontargeted tissue lipidomics using liquid chromatography-mass spectrometry. *J. Pharm. Biomed. Anal.* **2020**, *190*, 113520. [CrossRef] [PubMed]
44. Meng, Q.; Hu, X.; Zhao, X.; Kong, X.; Meng, Y.M.; Chen, Y.; Su, L.; Jiang, X.; Qiu, X.; Huang, C.; et al. A circular network of coregulated sphingolipids dictates lung cancer growth and progression. *eBioMedicine* **2021**, *66*, 103301. [CrossRef] [PubMed]
45. Hu, T.; Han, F.; An, Z. Comprehensive profiling of serum glycosphingolipids to discover the diagnostic biomarkers of lung cancer and uncover the variation of glycosphingolipid networks in different lung cancer subtypes. *Anal. Methods* **2024**, *16*, 7873–7887. [CrossRef] [PubMed]
46. Fan, T.W.M.; Zhang, X.; Wang, C.; Yang, Y.; Kang, W.-Y.; Arnold, S.; Higashi, R.M.; Liu, J.; Lane, A.N. Exosomal lipids for classifying early and late stage non-small cell lung cancer. *Anal. Chim. Acta* **2018**, *1037*, 256–264. [CrossRef] [PubMed]
47. Smolarz, M.; Kurczyk, A.; Jelonek, K.; Żyła, J.; Mielańczyk, Ł.; Sitkiewicz, M.; Pietrowska, M.; Polańska, J.; Rzyman, W.; Widłak, P. The Lipid Composition of Serum-Derived Small Extracellular Vesicles in Participants of a Lung Cancer Screening Study. *Cancers* **2021**, *13*, 3414. [CrossRef] [PubMed]
48. Yang, Q.; Luo, J.; Xu, H.; Huang, L.; Zhu, X.; Li, H.; Yang, R.; Peng, B.; Sun, D.; Zhu, Q.; et al. Metabolomic investigation of urinary extracellular vesicles for early detection and screening of lung cancer. *J. Nanobiotechnol.* **2023**, *21*, 153. [CrossRef] [PubMed]
49. Hao, D.; Sengupta, A.; Ding, K.; Ubeydullah, E.R.; Krishnaiah, S.; Leighl, N.B.; Shepherd, F.A.; Seymour, L.; Weljie, A. Metabolites as Prognostic Markers for Metastatic Non-Small Cell Lung Cancer (NSCLC) Patients Treated with First-Line Platinum-Doublet Chemotherapy. *Cancers* **2020**, *12*, 1926. [CrossRef] [PubMed]

50. Jiang, H.; Li, X.S.; Yang, Y.; Qi, R.X. Plasma lipidomics profiling in predicting the chemo-immunotherapy response in advanced non-small cell lung cancer. *Front. Oncol.* **2024**, *14*, 1348164. [CrossRef] [PubMed]
51. Takanashi, Y.; Kahyo, T.; Sekihara, K.; Kawase, A.; Setou, M.; Funai, K. Prognostic potential of lipid profiling in cancer patients: A systematic review of mass spectrometry-based studies. *Lipids Health Dis.* **2024**, *23*, 154. [CrossRef] [PubMed]
52. Hanahan, D.; Weinberg, R.A. Hallmarks of cancer: The next generation. *Cell* **2011**, *144*, 646–674. [CrossRef] [PubMed]
53. Pavlova, N.N.; Thompson, C.B. The Emerging Hallmarks of Cancer Metabolism. *Cell Metab.* **2016**, *23*, 27–47. [CrossRef] [PubMed]
54. Vander Heiden, M.G.; DeBerardinis, R.J. Understanding the Intersections between Metabolism and Cancer Biology. *Cell* **2017**, *168*, 657–669. [CrossRef] [PubMed]
55. Snaebjornsson, M.T.; Janaki-Raman, S.; Schulze, A. Greasing the Wheels of the Cancer Machine: The Role of Lipid Metabolism in Cancer. *Cell Metab.* **2020**, *31*, 62–76. [CrossRef] [PubMed]
56. Jin, H.-R.; Wang, J.; Wang, Z.-J.; Xi, M.-J.; Xia, B.-H.; Deng, K.; Yang, J.-L. Lipid metabolic reprogramming in tumor microenvironment: From mechanisms to therapeutics. *J. Hematol. Oncol.* **2023**, *16*, 103. [CrossRef] [PubMed]
57. Kanehisa, M.; Sato, Y.; Furumichi, M.; Morishima, K.; Tanabe, M. New approach for understanding genome variations in KEGG. *Nucleic Acids Res.* **2019**, *47*, D590–D595. [CrossRef] [PubMed]

Disclaimer/Publisher's Note: The statements, opinions and data contained in all publications are solely those of the individual author(s) and contributor(s) and not of MDPI and/or the editor(s). MDPI and/or the editor(s) disclaim responsibility for any injury to people or property resulting from any ideas, methods, instructions or products referred to in the content.